Mathematical Medicine and Biology: A Journal of the IMA (2022) **00**, 1–30
https://doi.org/10.1093/imammb/dqac001

Deterministic and stochastic in-host tuberculosis models for bacterium-directed and host-directed therapy combination

Wenjing Zhang*
Department of Mathematics and Statistics, Texas Tech University Lubbock, TX 79409-1042, USA
*Corresponding author. Email: wenjing.zhang@ttu.edu

[Received on 16 February 2021; revised on 22 November 2021; accepted on 27 January 2022]

Mycobacterium tuberculosis (TB) infection can involve all immune system components and can result in different disease outcomes. The antibiotic TB drugs require strict adherence to prevent both disease relapse and mutation of drug- and multidrug-resistant strains. To overcome the constraints of pathogen-directed therapy, host-directed therapy has attracted more attention in recent years as an adjunct therapy to enhance host immunity to fight against this intractable pathogen. The goal of this paper is to investigate in-host TB models to provide insights into therapy development. Focusing on therapy-targeting parameters, the parameter regions for different disease outcomes are identified from an established ODE model. Interestingly, the ODE model also demonstrates that the immune responses can both benefit and impede disease progression, depending on the number of bacteria engulfed and released by macrophages. We then develop two Itô SDE models, which consider the impact of demographic variations at the cellular level and environmental variations during therapies along with demographic variations. The SDE model with demographic variation suggests that stochastic fluctuations at the cellular level have significant influences on (1) the T-cell population in all parameter regions, (2) the bacterial population when parameters located in the region with multiple disease outcomes and (3) the uninfected macrophage population in the parameter region representing active disease. Further, considering environmental variations from therapies, the second SDE model suggests that disease progression can slow down if therapies (1) can have fast return rates and (2) can bring parameter values into the disease clearance regions.

Keywords: in-host tuberculosis model; deterministic model; stochastic model; bifurcation analysis.

1. Introduction

Tuberculosis (TB) is a major cause of death from infectious diseases globally. It infects one quarter of the world population and claims 1.4 million lives per year (Perelson & Nelson, 1999). Even though it is an ancient disease, TB is still formidable due to the spread of drug-resistant strains, which can lead to re-emergence in the regions of the world with smaller TB burdens. The world is at a critical tipping point in the elimination of TB (World Health Organization, 2020). The primary strategies to fight against TB are rapid identification, appropriate treatment of infected cases and continued surveillance to manage outbreaks. It is necessary to incorporate interventions at the population level with a decrease in the disease progression at the individual level.

On an individual basis, the disease outcome varies among clearance, active disease and latent tuberculosis infection (LTBI) (Gupta *et al.*, 2009; Meng *et al.*, 2020). In more detail, after the exposure with Mycobacterium tuberculosis (Mtb), a fraction of individuals can eradicate the infecting Mtb pathogens naturally and achieve early clearance. Evidence of early clearance in Uganda (Bisset *et al.*, 2004) ranges from 3.4% to 23.8% (Conde & Lapa e Silva, 2011). Another roughly 5%–10% of infected

individuals rapidly progress to active disease (fast progression) (Alexander & Wahl, 2011) after initial exposure, while the majority of infected individuals stay in LTBI status (Allen, 1999). The global prevalence of LTBI is estimated about 25% (de Martino *et al.*, 2019). Patients with LTBI status have Mtb pathogens present but show no clinical symptoms. However, endogenous reactivation (slow progression) can still induce disease progression to active TB for the rest of their life at about 5%–10% (Perelson & Nelson, 1999). Moreover, even though only about one in ten LTBI cases become active, this progression contributes to approximately 80% of active disease cases globally (Smith, 2003). One of the causes of different disease outcomes and disease progression is an impaired host immune system, particularly in the case of immune suppression by HIV and malnutrition. For HIV-infected individuals, the damage to the innate immunity increases macrophage turnover (Liu *et al.*, 2006), and the impairment of adaptive immune system reduces CD4+ T-cell counts and the baseline monocyte to lymphocyte ratio (Uplekar *et al.*, 2015). For malnourished TB patients (such as vitamin D deficiency), delayed recovery and higher mortality rates are reported (Lin & Flynn, 2010).

The development of the antibiotic TB medication streptomycin started in 1943 (Cobat *et al.*, 2009). Nowadays, LTBI and active TB disease can be treated. The anti-TB drug treatments include four first-line drugs, isoniazid (INH), rifampin (RIF), pyrazinamide (PZA) and ethambutol (EMB), which either act as a bactericide or a bacteriostatic agent. Even though the anti-TB regimens have an up-to-95% efficacy (Dhooge *et al.*, 2003), treatment effectiveness differs according to the adherence of strict routine conditions (Naranbhai *et al.*, 2013). If patients stop using medications too soon, take incorrect medication or use irregular medication, the Mtb bacteria may still live, which can cause disease relapse and mutation of antibiotic-resistant strains. The antibiotic-resistant Mtb strains are much more difficult to treat. Frustrated by antimicrobial resistance and strict treatment adherence, researchers have focused on host-cell factors to inhibit Mtb pathogens' replication or persistence and promote host immune responses against the invading pathogens.

Host-directed therapies (HDTs) are emerging as adjunctive therapies lately (Zumla *et al.*, 2020). HDTs aim at the enhancement of long-term treatment outcome and the functional cure of persistent Mtb bacteria. Examples of adjunctive HDTs include (1) nonsteroidal anti-inflammatory drugs, such as ibuprofen, to prevent host inflammatory responses; (2) vitamins and dietary supplements, such as vitamin D, to promote immune response; (3) and other drugs to reduce intracellular bacillary load of Mtb (Zumla *et al.*, 2015). To facilitate the development of novel therapy strategies, identification of the key mechanisms of the interactions between Mtb bacteria and host immune response is crucial. This serves as the motivation of this project.

Mathematical modelling has been a fundamental research tool for studying complex dynamics and identifying the underlying causal factors. The papers Wigginton & Kirschner (2001), Martineau *et al.* (2007), Gupta *et al.* (2009) and Alexander & Wahl (2011) are starts of in-host modelling regarding immunology of Mtb infections and host-immune response. These previous works successfully combined both bacterial and immune response mechanisms and developed models of Mtb-host interactions to identify the key factors for various disease outcomes through deterministic models. The study of how stochastic variations affecting in-host dynamics has still fallen short. This may be due to the high model complexity. The previous in-host modelling work contains a large number of equations and parameters, which put a big challenge on the identification of significant model parameters driving the disease progression.

In this project, we adopt an established in-host TB infection model (Gammack *et al.*, 2005), which incorporates the essential bacterial and immune response mechanisms in a 4D deterministic system with 18 parameter values and successfully generates all disease outcomes including clearance, LTBI and active disease. In this contribution, however, Du *et al.* employed and analysed only an asymptotic

version of the model that neglects the effects of the CD4 T-cell population. Then, the papers Zhang (2020) and Zhang *et al.* (2021, 2020) present rigourous mathematical analyses on a reduced model and the original full model, respectively. In this paper, we focus on the driving factors and consider the stochastic variations on demographic variables (including Mtb pathogen and immune cells populations) and on environmental variables (including the identified driving factors) to explore their influences on disease progression.

The paper is organized as follows. In the rest of Section 1, we present an established deterministic Mtb-host model and its basic mathematical properties. In Section 2, we formulate two stochastic models considering demographic variations and environmental variations. In Section 3, we delimit the parameter regions according to different disease outcomes through bifurcation analysis. We further demonstrate the stochastic influences on each parameter region. In Section 4, we investigate the speed of the disease progression under combination therapies. The paper ends with a conclusion and discussion in Section 5.

1.1 *Mtb-host dynamics*

Mtb infection most frequently happens in the respiratory tract, particularly the lung (pulmonary TB), and the regional lymph nodes. When Mtb are inhaled into the lungs and taken up by resident alveolar macrophages, these bacteria start to multiply and make alveolar macrophages their main target. If receiving adequate stimulation for activation, macrophages can effectively ingest and destroy their phagocytized bacteria. Otherwise, the phagocytized bacteria reproduce inside their host macrophages. The host macrophages are eventually unable to be activated due to the increased phagocytized bacteria load and become chronically infected. The chronically infected macrophages, which are unable to kill their intracellular bacteria, ultimately either undergo programmed cell death (i.e. apoptosis or necrosis) due to an excessive intracellular bacterial load or are destroyed through T-cell-mediated immune responses. Both processes lead to the death of chronically infected macrophages, which release intracellular bacteria to the extracellular environment. These extracellular bacteria again are engulfed by activated macrophages and result in either bacterial elimination or chronically infected macrophages. The initiation of the T-cell-mediated immunity starts from the infected front-line innate immune cells, including macrophages and dendritic cells. These innate immune cells migrate from the lung to the draining lymph node and activate naive T cells with the present of Mtb. Activated effector and memory T cells then travel back to the lung infection site, engage in granuloma formation and control the infection. The major elements of the host immune response against Mtb infection involve macrophages, T lymphocytes and Mtb bacteria.

1.2 *In-host deterministic model*

Our model describes the host-pathogen dynamics for human Mtb infection in lung tissue. Since the site of infection is the human lung, we focus on the interactions among Mtb bacteria (the pathogens), macrophages (Mtb ideal target cells) and lymphocytes (especially T cells for cell-mediated, cytotoxic adaptive immunity). The measurement for all cells is taken in units per millilitre. The 4D model (1.1) describes the dynamics of the uninfected M_u and infected M_i macrophages, the Mtb bacteria B and the CD4+ T cells T. In this model, we consider the effects from CD8+ T cells (cytotoxic T cells or CTL) and cytokines indirectly. The model was developed by Gammack *et al.* (2005) and analysed by Zhang *et al.* (2021, 2020). We present the model in (1.1) followed by model descriptions. Moreover, we write

TABLE 1 *Parameter symbol, descriptions and values (source: Wigginton & Kirschner, 2001; Martineau et al., 2007; Gupta et al., 2009; Gammack et al., 2005).*

Symbol	Description (unites)	Value
s_M	Recruitment rate of M_u (1/ml day)	5000
s_T	Recruitment rate of T (1/ml day)	6.6
μ_M	Death rate of M_u (1/day)	0.01
b	Loss rate of M_i (1/day)	0.11
μ_T	Death rate of T (1/day)	0.33
β	Infection rate by B (1/day)	2×10^{-7}
η	Bacteria killing rate by M_u rate (1/ml day)	1.25×10^{-8}
γ	Cell-mediated immunity rate (1/day)	1.5
δ	Proliferation rate of B (1/day)	5×10^{-4}
c_M	Expansion rate of T induce by M_i (1/day)	10^{-3}
c_B	Expansion rate of T induce by B (1/day)	5×10^{-3}
e_M	Saturating factor of T expansion related to M_i	10^{-4}
e_B	Saturating factor of T expansion related to B	10^{-4}
c	Half-saturation ratio for M_i lysis (T/M_i)	3
K	Carrying capacity of B (1/ml)	10^8
N_1	Max MOI of M_i (B/M_i)	50
N_2	Max no. of B released by apoptosis (and necrosis) (T/M_i)	20
N_3	$N_3 = N_1/2$ (B/M_i)	25

the parameter descriptions and values in Table 1.

$$\begin{aligned}
\frac{dM_u}{dt} &= s_M - \mu_M M_u - \beta M_u B \\
\frac{dM_i}{dt} &= \beta M_u B - bM_i - \gamma M_i \frac{T/M_i}{T/M_i + c} \\
\frac{dB}{dt} &= \delta B\left(1 - \frac{B}{K}\right) + M_i\left(N_1 b + N_2 \gamma \frac{T/M_i}{T/M_i + c}\right) - M_u B(\eta + N_3\beta) \\
\frac{dT}{dt} &= s_T + \frac{c_M M_i T}{e_M T + 1} + \frac{c_B B T}{e_B T + 1} - \mu_T T.
\end{aligned} \tag{1.1}$$

Macrophages. Uninfected M_u macrophages arrive at the infection site at a constant recruitment rate of s_M and have a finite lifespan with a natural death rate μ_M. With the presence of Mtb, uninfected macrophages engulf the bacteria B and become chronically infected at a rate β without receiving sufficient stimulation for activation. The apoptosis and necrosis of infected macrophages could occur naturally, by bursting induced by the excessive intracellular bacterium load caused by the phagocytized bacteria multiplication, or by receiving the death signal from CD8+ cells. The loss rate of infected macrophages due to natural death and bursting is denoted as b.

Since the activation and proliferation of CD8+ T cells require the signal from CD4+ T cells, we consider the cytotoxic action (i.e. CD8+ T cells target intracellular bacteria) is proportional to CD4+ T cell function. Therefore, the ratio of CD4+ T cell to infected macrophage (T/M_i) determines the rate of

CD8+ T cells killing infected macrophages (M_i). This rate reaches to its half-maximum at the value of c and its maximum at γ.

Bacteria. The bacterial population in TB infection consists of intracellular and extracellular bacteria. Extracellular bacteria become intracellular or phagocytized through engulfment by a host macrophage. Intracellular bacteria are released and become extracellular when infected macrophages undergo programmed cell death or killed by T cells. We define extracellular bacteria as B, whose division is governed by a logistic term $\delta B(1 - B/K)$ with a constant growth rate δ and a maximal carrying capacity K. The death of an infected macrophage releases N_1 intracellular bacteria per cell due to natural death and cell bursting and releases N_2 intracellular bacteria per cell due to CD8+ T cell cytotoxic action. With adequate stimulation, uninfected macrophage engulfment can kill the phagocytized bacteria ($\eta M_u B$, assuming the killing rate is η). Otherwise, phagocytosis turns uninfected macrophages into chronically infected ($N_3 \beta B M_u$). We assume the engulfment process takes N_3 bacteria per macrophage cell.

CD4+ T lymphocytes. CD4+ T cells play a role in signalling CD8+ T cell activation and replication to eliminate infected macrophages via cytotoxic action. CD4+ T cells also produce cytokines for granuloma formation and infection control. During the TB infection, professional antigen-presenting cells, including macrophages and dendritic cells, travel to lung-draining lymph node to present Mtb antigens to naive T cells and activate them. We assume that CD4+ T cells are activated by (1) infected macrophages with phagocytized bacteria at rate c_M with the saturating factor e_M and (2) dendritic cells (assumed in proposition to the extracellular bacteria) at rate c_B with the saturating factor e_B. The natural recruitment and death rates of CD4+ T cells are denoted as s_T and μ_T.

1.3 *Basic properties of the deterministic model*

As an airborne disease, TB is transmitted from person to person through airborne particles containing Mtb (i.e. droplet nuclei). The invasion of the infecting Mtb produces immune responses in the host. Early clearance can be achieved if an effective innate immune response successfully eradicate the infecting Mtb before the development of an adaptive response. Otherwise, the infection stays and develops to either an active TB or LTBI. A delayed clearance can still be achieved thanks to adaptive immune responses.

In the previous paper Zhang *et al.* (2020), we proved that the solution trajectories stay in a bounded positive quadrant for all positive time and carried out the steady state analysis. We denote the steady state as $(\bar{M}_u, \bar{M}_i, \bar{B}, \bar{T})$. If uninfected macrophages phagocytose all extracellular Mtb and kill all the engulfed bacteria through phagocytosis, then no chronically infected macrophages will be generated, and the early infection is eradicated. That means the infection term ($\beta M_u B$) is $\frac{s_M}{\mu_M+\beta B} B\beta \frac{1}{b+\gamma} = M_i = 0$. We then have $B = 0$. Here, $s_M/(\mu_M + \beta B)$ denotes the uninfected macrophage population on a quasi-steady state level, $1/(b + \gamma)$ is the minimum average lifetime of an infected macrophage (b the loss rate of infected macrophages and γ the maximum infected macrophage elimination rate by T-cell-mediated immune response). The infection then reaches a trivial steady state, $(\bar{M}_{u0}, \bar{M}_{i0}, \bar{B}_0, \bar{T}_0) = (s_M/\mu_M, 0, 0, s_T/\mu_T)$. It denotes the clearance of resident bacteria by macrophages with the help of T-cell-mediated immune response. If $\frac{s_M}{\mu_M+\beta B} B\beta \frac{1}{b+\gamma} = M_i \neq 0$, the existence of bacteria located anywhere other than inside infected macrophages is possible. This infected steady state is $\bar{M}_u = \frac{s_M}{\mu_M+\beta B}$, $\bar{T} = \frac{\beta B \bar{M}_u - b\bar{M}_i}{\beta B \bar{M}_u - (b+\gamma)\bar{M}_i} c\bar{M}_i$, $\bar{M}_i = \left(\frac{B\delta}{K} - \frac{\delta + s_M[(N_2-N_3)\beta-\eta]}{\beta B+\mu_M}\right) \frac{B}{b(N1-N2)}$, and $F(B) = -e_B e_M \mu_T \bar{T}^3 + \left[(c_M\bar{M}_i + e_M s_T - \mu_T)e_B + e_M(c_B B - \mu_T)\right]\bar{T}^2 + \left[c_B B + c_M\bar{M}_i + (e_B + e_M)s_T - \mu_T\right]\bar{T} + s_T = 0$.

2. Two Stochastic Models

Randomness is a typical feature in immunology (Wodarz, 2007). It prevents us from foreseeing the exact state at a given time during the process of immune responses. However, if the same experiment is repeated a large number of times, we can obtain a certain trend with similar outcomes. For example, the solution of a linear deterministic model represents the expectation of the corresponding stochastic model. However, the solutions of deterministic models fail to provide information about the intrinsic variability in stochastic models. These random variations in immune responses could induce various disease and treatment outcomes in a model with multiple stable equilibriums. We apply multivariate Itô SDEs to model the dynamics of Mtb bacteria and immune cells' interaction by using the modelling algorithm based on a multivariate continuous Markov chain model (Allen *et al.*, 2020, 2008; Allen, 2007b, 2010; Arranz-Trullén *et al.*, 2017).

Two stochastic models are formulated based on demographic variations and environmental variations, respectively. The study of population changes of pathogens and immune cells can be viewed as the study of demography in population dynamics. The dynamics between pathogens and the immune system demonstrate predator–prey interactions. The immune cells, acting as predators, capture and kill their pathogen prey. During this interaction, the sizes of immune cell populations grow. This induces a faster decline in the pathogen population. In the meantime, Mtb pathogens proliferate and evolve survival strategies to avoid the predation from immune cells. Moreover, the infection process turns healthy macrophage cells into infected cells.

We model the changes over time within the cell population processes, such as proliferation, death, immigration and transition of both immune cells and Mtb bacteria as demographic variations. An SDE model with demographic variations captures the random nature of this cell population birth-death-immigration process. Moreover, the noise-induced demographic variations can cause species collapse/recover between high- and low-abundance equilibriums (Mitnick *et al.*, 2009) in the ecology system. Analogously, demographic variations could induce the transition between a low-infection state (such as LTBI) and a high-infection state (such as active disease) in the interplay of pathogens and immune system. In addition, the inhabiting environment (such as the individual's physical factors) also changes and very likely affects the pathogen and host immune cell populations in other random manners, such as the infected macrophage loss rate, cell-mediated immunity rate, macrophages bacteria killing rate and bacterial proliferation rate. Instead of including additional variables in the existing ODE model, an alternative way to include these environmental variations is modelling the affected parameters as random variables following certain stochastic processes (Allen *et al.*, 2020). These environmental variations happen especially in drug therapy and alter the cellular environment with random manner due to the heterogeneity in individual cell response. This motivates us to develop the second SDE model with both demographic and environmental variations.

2.1 *SDE model with demographic variations*

To formulate stochastic processes from the underling deterministic model (1.1), the first step is to identify the possible interactions resulting in population changes and their probabilities in a given small-time interval Δt. The summary of these changes is in Table 2. Let $\overrightarrow{X}(t) = (M_u, M_i, B, T)^{tr}$, $\Delta\overrightarrow{X} = \overrightarrow{X}(t+\Delta t) - \overrightarrow{X}(t)$ and $t \in (0, \infty)$. Notice that for the SDE model, it is not necessary to convert the units of continuous random variables, M_u, M_i, B and T, from concentration to population size (Antony *et al.*, 1993), since the changes $(\Delta\overrightarrow{X})_k$ do not need to be integer-valued. It is assumed that intracellular Mtb bacteria are reproduced with an infected macrophage and released only upon the

TABLE 2 *Possible state changes during Δt and their associated probabilities.*

k	State Change $(\Delta \overrightarrow{X})_k$	Probability $p_i \Delta t + o(\Delta t)$	Description
1	$(1,0,0,0)^{tr}$	$s_M \Delta t + o(\Delta t)$	M_u recruitment
2	$(-1,0,0,0)^{tr}$	$\mu_M M_u \Delta t + o(\Delta t)$	$M_u$death
3	$(-1,1,0,0)^{tr}$	$\beta M_u B \Delta t + o(\Delta t)$	M_u infected by B
4	$(0,-1,N_1,0)^{tr}$	$bM_i \Delta t + o(\Delta t)$	Loss of M_i and release bacteria
5	$(0,-1,N_2,0)^{tr}$	$\gamma M_i \frac{T/M_i}{T/M_i+c} \Delta t + o(\Delta t)$	$M_i$killed by cell-mediated immunity and release bacteria
6	$(0,0,1,0)^{tr}$	$\delta B(1-B/K)\Delta t + o(\Delta t)$	Mtb bacteria proliferation
7	$(0,0,-1,0)^{tr}$	$M_u B(\eta + N_3\beta)\Delta t + o(\Delta t)$	Extracellular loss due to M_i killing and phagotysis of Mtb
8	$(0,0,0,1)^{tr}$	$s_T \Delta t + o(\Delta t)$	T-cell recruitment
9	$(0,0,0,1)^{tr}$	$\frac{c_M M_i T}{e_M T+1} \Delta t + o(\Delta t)$	T-cell activated by M_i
10	$(0,0,0,1)^{tr}$	$\frac{c_B B T}{e_B T+1} \Delta t + o(\Delta t)$	T-cell activated by B
11	$(0,0,0,-1)^{tr}$	$\mu_T T \Delta t + o(\Delta t)$	T-cell death

lysis of the infected macrophage. If the death of one unit of the infected macrophage, denoted by -1, is due to the killing of the cell-mediated immunity, N_1 units of Mtb bacteria are released, $(\Delta \overrightarrow{X})_4 = (0,-1,N_1,0)^{tr}$. If it is caused by excessive intracellular bacterium load, N_2 units of Mtb bacteria are released, $(\Delta \overrightarrow{X})_5 = (0,-1,N_2,0)^{tr}$. Furthermore, a loss of extracellular Mtb bacteria can also be caused by phagocytosis of extracellular Mtb bacteria by uninfected macrophages, $(\Delta \overrightarrow{X})_7 = (0,0,-1,0)^{tr}$. All the possible changes in the small-time interval Δt include these eleven changes in Table 2 and a case of no change, $(\Delta \overrightarrow{X})_{12} = (0,0,0,0)^{tr}$, with the possibility $p_{12}\Delta t = 1 - \sum_{k=1}^{11} p_k \Delta t$. Notice that the higher order of Δt is neglected.

The stochastic processes are formed from the underling deterministic ODE model (1.1).

In the second step of formulation, omitting the higher-order terms of Δt, we compute the first-order approximation of the expectation $\mathbb{E}(\Delta \overrightarrow{X})$ and the covariance $\mathbb{E}[(\Delta \overrightarrow{X})(\Delta \overrightarrow{X})^{tr}]$. The approximated expectation of $\Delta \overrightarrow{X}$ can be expressed as follows:

$$\mathbb{E}\left(\Delta \overrightarrow{X}\right) = \sum_{k=1}^{11} p_k \Delta t \left(\Delta \overrightarrow{X}\right)_k = \overrightarrow{f}\ \left(M_u, M_i, B, T\right)\ \Delta t,$$

where

$$\overrightarrow{f} = \begin{pmatrix} f_1\left(M_u,M_i,B,T\right) \\ f_2\left(M_u,M_i,B,T\right) \\ f_3\left(M_u,M_i,B,T\right) \\ f_4\left(M_u,M_i,B,T\right) \end{pmatrix} = \begin{pmatrix} s_M - \mu_M M_u - \beta M_u B \\ \beta M_u B - bM_i - \gamma M_i \dfrac{T/M_i}{T/M_i + c} \\ \delta B\left(1-\dfrac{B}{K}\right) + M_i\left(N_1 b + N_2 \gamma \dfrac{T/M_i}{T/M_i+c}\right) - M_u B(\eta + N_3\beta) \\ s_T + \dfrac{c_M M_i T}{e_M T+1} + \dfrac{c_B B T}{e_B T+1} - \mu_T T. \end{pmatrix}$$

is the drift vector, which is the same as the right side of the deterministic ODE model (1.1). Here, p_is are coefficients of the Δt terms of the probabilities for the eleven events in Table 2.

The covariance matrix is a 4×4 matrix, $\mathbb{E}[(\Delta \overrightarrow{X})(\Delta \overrightarrow{X})^{tr}] - \mathbb{E}(\Delta \overrightarrow{X})[\mathbb{E}(\Delta \overrightarrow{X})]^{tr}$. Dropping the $(\Delta t)^2$ order term $\mathbb{E}(\Delta \overrightarrow{X})[\mathbb{E}(\Delta \overrightarrow{X})]^{tr}$ results the approximation to order Δt as follows:

$$\mathbb{E}[(\Delta \overrightarrow{X})(\Delta \overrightarrow{X})^{tr}] \approx \sum_{k=1}^{11} p_k \Delta t \left(\Delta \overrightarrow{X}\right)_k \left(\Delta \overrightarrow{X}\right)_k^{tr} = \Sigma\left(M_u, M_i, B, T\right) \Delta t.$$

Here, the matrix Σ takes the following form:

$$\Sigma = \begin{bmatrix} p_1+p_2+p_3 & -p_3 & 0 & 0 \\ -p_3 & p_3+p_4+p_5 & -N_1p_4-N_2p_5 & 0 \\ 0 & -N_1p_4-N_2p_5 & N_1^2p_4+N_2^2p_5+p_6+p_7 & 0 \\ 0 & 0 & 0 & p_8+p_9+p_{10}+p_{11} \end{bmatrix} = \left[\Sigma_{i,j}\right]$$

The nonzero elements of Σ are as follows:

$$\begin{aligned}
&\Sigma_{11} = BM_u\beta + M_u\mu_M + s_M, \qquad \Sigma_{12} = -\beta M_u B, \\
&\Sigma_{21} = -\beta M_u B, \Sigma_{22} = \beta M_u B + bM_i + \gamma M_i \frac{T/M_i}{T/M_i + c}, \\
&\Sigma_{23} = -bM_iN_1 - \gamma M_i \frac{T/M_i}{T/M_i + c} N_2, \\
&\Sigma_{32} = -bM_iN_1 - \gamma M_i \frac{T/M_i}{T/M_i + c} N_2, \\
&\Sigma_{33} = bM_iN_1^2 + \gamma M_i \frac{T/M_i}{T/M_i + c} N_2^2 + \delta B\left(1 - \frac{B}{K}\right) + M_uB(N_3\beta + \eta) \\
&\Sigma_{44} = s_T + c_MM_i\frac{T}{Te_M + 1} + c_BB\frac{T}{Te_B + 1} + \mu_T T.
\end{aligned}$$

Instead of computing the square root of Σ to find the diffusion matrix, we calculate a matrix $B\left(M_u, M_i, B, T\right) = [B_{i,j}]_{4\times 11}$, such that $BB^{tr} = \Sigma$. In the matrix B, four rows indicate four state variables (M_u, M_i, B and T), eleven columns represent eleven events in Table 2. The nonzero elements in the matrix B are as follows:

$$\begin{aligned}
&B_{11} = \sqrt{s_M}, \quad B_{12} = -\sqrt{\mu_M M_u}, \quad B_{13} = -\sqrt{\beta M_u B}, \\
&B_{23} = \sqrt{\beta M_u B}, \quad B_{24} = -\sqrt{bM_i}, \quad B_{25} = -\sqrt{\frac{\gamma M_i T}{M_i c + T}}, \\
&B_{34} = N_1\sqrt{(bM_i)}, \quad B_{35} = N_2\sqrt{\frac{\gamma M_i T}{M_i c + T}}, \quad B_{36} = \sqrt{\delta B(1 - \frac{B}{K})}, \quad B_{37} = -\sqrt{M_uB(N_3\beta + \eta)}, \\
&B_{48} = \sqrt{s_T}, \quad B_{49} = \sqrt{\frac{c_MM_iT}{Te_M + 1}}, \quad B_{4,10} = \sqrt{\frac{c_BBT}{Te_B + 1}}, \quad B_{4,11} = -\sqrt{\mu_T T}.
\end{aligned}$$

The Itô SDE model considering the demographic variations has the following form:

$$\begin{cases} dM_u(t) &= f_1(M_u, M_i, B, T)dt + B_{11}dW_1(t) + B_{12}dW_2(t) + B_{13}dW_3(t), \\ dM_i(t) &= f_2(M_u, M_i, B, T)dt + B_{23}dW_3(t) + B_{24}dW_4(t) + B_{25}dW_5(t), \\ dB(t) &= f_3(M_u, M_i, B, T)dt + B_{34}dW_4(t) + B_{35}dW_5(t) + B_{36}dW_6(t) + B_{37}dW_7(t), \\ dT(t) &= f_4(M_u, M_i, B, T)dt + B_{48}dW_8(t) + B_{49}dW_9(t) + B_{4,10}dW_{10}(t) + B_{4,11}dW_{11}(t), \\ \overrightarrow{X}(0) &= \left(M_u(0), M_i(0), B(0), T(0)\right), \end{cases} \tag{2.1}$$

where the vector $W_i(t)$, $i = 1 \ldots 11$ are eleven independent Wiener processes, and f_i, $i = 1 \ldots 4$ are four elements in the drift vector $\overrightarrow{f}(M_u, M_i, B, T)$.

2.2 *SDE model with demographic and environmental variations*

HDTs can modulate host immune pathways. The therapies can also affect the corresponding parameters with random manner. We model these environmental effects by including additional random variables in the SDE model (2.1).

In previous work Zhang *et al.* (2021), we identify four parameters, which significantly affect the disease progression. These four parameters are the bacterial proliferation rate δ, the infected macrophages' loss rate b, the cell-mediated immunity rate γ and macrophages' killing rate η. We then consider environmental variations on them. We adopt a mean-reverting process (Allen, 2017; Antony *et al.*, 1993), which was modelled to study drug administrations and was shown to fit well with real data. Let $\overrightarrow{C}(t) = \left(C_1(t), C_2(t), C_3(t), C_4(t)\right)^{tr}$, where $C_1(t) = \delta(t)$, $C_2(t) = b(t)$, $C_3(t) = \gamma(t)$ and $C_4(t) = \eta(t)$, $C_s = (C_{s1}, C_{s2}, C_{s3}, C_{s4}) = (\delta_s, b_s, \gamma_s, \eta_s)$ and $C_0 = (C_{01}, C_{02}, C_{03}, C_{04}) = (\delta_0, b_0, \gamma_0, \eta_0)$, we assume the vector $\overrightarrow{C}(t)$ is a vector of continuous, mean-reverting, stochastic processes. Each element of $\overrightarrow{C}(t)$ satisfies an Itô stochastic differential equation as follows:

$$C_i(t) = \alpha_i(C_{si} - C_i(t))dt + \sigma_i C_i(t)dW_{ei}(t), \quad \text{for } i = 1, 2, 3, 4,$$

where $\alpha_i > 0$ is the return rate to the mean concentration C_{si}. Here, C_{si} denotes the desired therapy result, which is modulated by drug therapies. The timescale for $(C_{si} - C_i(t))$ returning to one half of its original level is $ln(2)/\alpha_i$. Therefore, a larger return rate value α_i implies a shorter return time to the desired therapy outcome. Parameters α_i and C_{si} can be tuned through drug administration strategies. Moreover, σ_i denotes the variability of the corresponding process and $W_e(t) = (W_{e1}(t), W_{e2}(t), W_{e3}(t), W_{e4}(t))$ is a vector of four independent Wiener processes. The asymptotic mean and variance of C_i are derived by Allen (2017) and Antony *et al.* (1993) as follows:

$$\lim_{t\to\infty} \mathbb{E}(C_i(t)|C_{0i}) = C_{si} \text{ and } \lim_{t\to\infty} Var(C_i(t)|C_{0i}) = \frac{C_{si}^2\sigma_i^2}{2\alpha_i - \sigma_i^2} \text{ for } \alpha_i > \frac{\sigma_i^2}{2};\ \infty \text{ for } \alpha_i \leqslant \frac{\sigma_i^2}{2}.$$

Therefore, to avoid a large variability and maintain a steady-state rate of immunity in therapies, the return rate should be sufficiently large, such that $\alpha_i > \frac{\sigma_i^2}{2}$. For the simulations in the next section, we assume $\alpha_i = 2\sigma_i^2$, which yields $\lim_{t\to\infty} Var(C_i(t)|C_{0i}) = \frac{C_{si}^2}{3}$. Therefore, under this assumption, the limiting mean and variance are independent of the return rate α_i, but only associated with the mean rate C_{si}.

The system of Itô SDEs with both demographic and environmental variations is written as follows:

$$\begin{cases} dM_u(t) &= f_1 dt + B_{11} dW_1(t) + B_{12} dW_2(t) + B_{13} dW_3(t), \\ dM_i(t) &= f_2 dt + B_{23} dW_3(t) + B_{24} dW_4(t) + B_{25} dW_5(t), \\ dB(t) &= f_3 dt + B_{34} dW_4(t) + B_{35} dW_5(t) + B_{36} dW_6(t) + B_{37} dW_7(t), \\ dT(t) &= f_4 dt + B_{48} dW_8(t) + B_{49} dW_9(t) + B_{4,10} dW_{10}(t) + B_{4,11} dW_{11}(t), \\ d\delta(t) &= \alpha_1(\delta_s - \delta(t))dt + \sigma_1 \delta(t) dW_{e1}(t), \\ db(t) &= \alpha_2(b_s - b(t))dt + \sigma_2 b(t) dW_{e2}(t), \\ d\gamma(t) &= \alpha_3(\gamma_s - \gamma(t))dt + \sigma_3 \gamma(t) dW_{e3}(t), \\ d\eta(t) &= \alpha_4(\eta_s - \eta(t))dt + \sigma_4 \eta(t) dW_{e4}(t), \end{cases} \tag{2.2}$$

where $f_i = f_i(M_u(t), M_i(t), B(t), T(t), \delta(t), b(t), \gamma(t), \eta(t))$, and $B_{i,j} = B_{i,j}(M_u(t), M_i(t), B(t), T(t), \delta(t), b(t), \gamma(t), \eta(t))$, for $i = 1...4$ and $j = 1..11$. Here, $\left(M_u(0), M_i(0), B(0), T(0), \delta_0, b_0, \gamma_0, \eta_0\right)$ denotes initial conditions, and $W_i(t)$ and $W_{ej}(t)$, $i = 1, ..., 11$ and $j = 1, ..., 4$ denote independent Wiener processes.

In the following section, numerical methods are used to approximate the solutions of the proposed SDE models. In our simulations, we apply a straightforward Euler–Maruyama method and set zero as an absorbing state.

3. Mtb-host Dynamics of the ODE Model and SDE Model with Demographic Variation

Mtb pathogens are extremely adaptive within a host. Their survival strategies involve multiple underlying mechanisms. Among these mechanisms, we focus on the bacterial proliferation rate δ, which is the parameter most affected by the first-line antibiotic drugs. We apply numerical bifurcation analyses to delimit the parameter space into four regions. Then we investigate disease clearance, latent infection and active disease on the ODE model (1.1) in the four identified parameter regions. Furthermore, we study the stochastic fluctuation in cellular levels in each parameter region through approximated stationary distributions from simulations of the SDE model (2.1).

3.1 *Multiple disease outcomes derived from bifurcation analysis*

Bacterial concentration reflects the local bacterial load, which is an important variable associated with Mtb virulence (Sud, 2006). The relation between bacterial concentration and its proliferation rate δ is demonstrated through a 1D bifurcation diagram in Fig. 1(a). The trivial steady state denoting disease clearance, $(\bar{M}_{u0}, \bar{M}_{i0}, \bar{B}_0, \bar{T}_0) = (s_M/\mu_M, 0, 0, s_T/\mu_T)$, exists for all positive values of δ. But it loses its stability when δ increases and crosses a branching point (BP) bifurcation (transcritical bifurcation) at $\delta_{BP} = 0.2956$ /day, where

$$(\bar{M}_{u0}, \bar{M}_{i0}, \bar{B}_0, \bar{T}_0) = (5 \times 10^5, 0, 0, 20) \quad \text{cells/ml}. \tag{3.1}$$

Without infection, a reference value for activated antigen-specific CD4+ T cells expressing CD25 is reported as $7 - 52$ cells/ml (Chakraborti, 2011), and a reference value for resting and activated macrophages is in the order of 10^5 cells/ml (Bark *et al.*, 2017; Schwartz *et al.*, 2020). The BP bifurcation

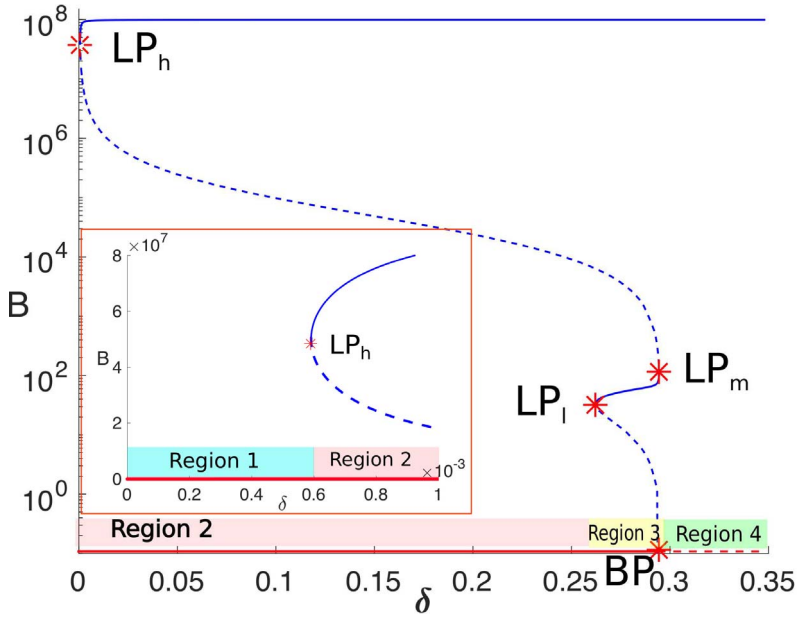

(a) Bifurcation diagram of B vs δ.

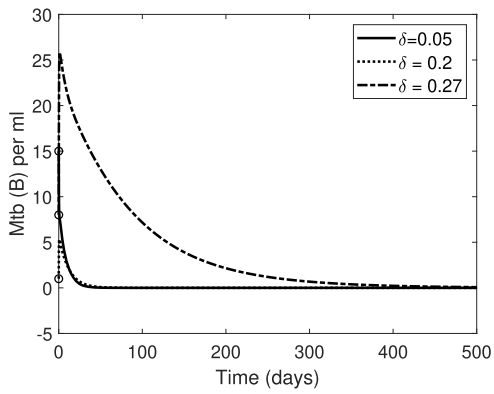

(b) Simulated disease clearance.

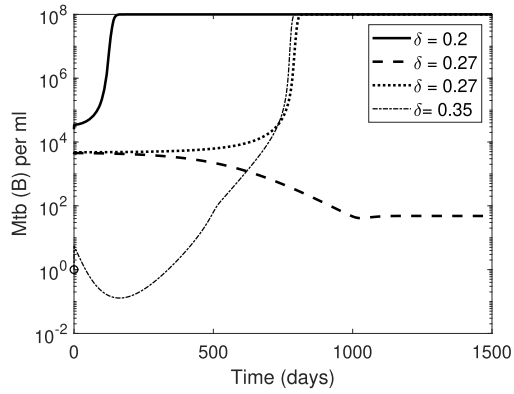

(c) Simulated LTBI and active disease.

FIG. 1. Bacterial concentrations under various bacterial proliferation rate. (a) Bifurcation diagram of the Mtb concentration (B per ml) vs the Mtb proliferation rate (δ per day). Region 1 is demonstrated in a closeup with $\delta \in (0, 1 \times 10^{-3})$. Sub-figures (b) and (c) demonstrate simulated clearance, LTBI and active disease. Parameter values are chosen as $\delta = 0.05$ in Region 1, $\delta = 0.2$ in Region 2, $\delta = 0.27$ in Region 3 and $\delta = 0.35$ in Region 4. Notice that simulated trajectories with $\delta = 0.2$ and $\delta = 0.27$ demonstrate multiple stable steady states. We circle the point $B(0)$ for four trajectories in (b) and (c) and take the other parameter values from Table 1.

generates a disease established steady state ($\bar{M}_u$, $\bar{M}_i$, $\bar{B}$, $\bar{T}$), which denotes the case that intracellular Mtb escape macrophages killing and become extracellular. The bacterial concentration can stabilize at a lower level around $10^1 - 10^2$ cells/ml, if δ takes a value between two saddle node (LP) bifurcations LP_l and LP_m. The bacterial concentration can also reach a high-level range $10^7 - 10^8$ cells/ml, if δ takes

a value between the saddle-node bifurcation LP_h and the transcritical bifurcation BP. A summary is as follows.

- Bistability happens between LP_h and LP_l. Taking $\delta = 0.2 \in [\delta_h, \delta_l]$, for instance, clearance occurs if the initial infection contains a low-level of Mtb bacteria, illustrated by the dotted curve (with $M_u(0) = 1 \times 10^6$, $M_i(0) = 1$, $B(0) = 1$ and $T(0) = 40$) in Fig. 1(b). Active disease happens in the case of a high level of bacteria in the initial infection, represented by the solid curve (with $M_u(0) = 3 \times 10^6$, $M_i(0) = 2 \times 10^3$, $B(0) = 2.5 \times 10^4$ and $T(0) = 3.7 \times 10^6$) in Fig. 1 (c).
- Triple stable steady states occur between LP_l and LP_m. Taking $\delta = 0.27 \in [\delta_l, \delta_m]$ for instance, disease clearance, LTBI and active disease are demonstrated by the dash-dot curve (with $M_u(0) = 6 \times 10^5$, $M_i(0) = 1$, $B(0) = 8$ and $T(0) = 90$) in Fig. 1(b), dashed curve (with $M_u(0) = 4.5 \times 10^6$, $M_i(0) = 270$, $B(0) = 4.2 \times 10^3$ and $T(0) = 7 \times 10^6$) in Fig. 1(c) and dotted curve (with $M_u(0) = 4.5 \times 10^6$, $M_i(0) = 270$, $B(0) = 4.8 \times 10^3$ and $T(0) = 7 \times 10^6$) in Fig. 1(c).
- The infection will certainly reach to a high-level if $\delta > \delta_m$, since $\delta_{BP} < \delta_m$. Taking $\delta = 0.35$ for example, a simulated trajectory starting from a low Mtb level and ending at high Mtb level, which is plotted in the dash-dot curve (with $M_u(0) = 1 \times 10^6$, $M_i(0) = 1$, $B(0) = 1$ and $T(0) = 40$) in Fig. 1(c).
- Disease clearance will certainly be achieved if $\delta < LP_h$, Taking $\delta = 0.05$, a simulated trajectory showing Mtb bacteria die out is the solid curve (with $M_u(0) = 1 \times 10^6$, $M_i(0) = 1$, $B(0) = 15$ and $T(0) = 40$) in Fig. 1(b).

The corresponding bifurcation points are LP_l: $(\bar{M}_u, \bar{M}_i, \bar{B}, \bar{T}, \delta_l) = (4.99672 \times 10^5, 2.366, 32.78, 40.16, 0.2621)$, LP_m: $(\bar{M}_u, \bar{M}_i, \bar{B}, \bar{T}, \delta_m) = (4.98848 \times 10^5, 7.171, 115.4, 7751, 0.2945)$ and LP_h: $(\bar{M}_u, \bar{M}_i, \bar{B}, \bar{T}, \delta_h) = (499.7, 3102, 4.997 \times 10^7, 0.7572 \times 10^{10}, 0.00059)$. Hopf bifurcation does not occur for the parameter values in Table 1. Moreover, saddle node bifurcation indicates the creation and destruction of equilibriums. Transcritical bifurcation, in this case, is the intersection of disease-free and infected equilibriums. These two bifurcations are sufficient to predict various disease outcomes, which include clearance, latent infection and active disease. We, therefore, do not consider higher codimension bifurcations in this project. Instead, we divide the parameter range of the bacterial proliferation δ into four regions shown in Fig. 1(a), i.e. Region 1: $[0, \delta_h]$, Region 2: $[\delta_h, \delta_l]$, Region 3: $[\delta_l, \delta_m]$ and Region 4: $[\delta_m, +\infty]$. In Region 1, only stable disease-free equilibrium exists. The ODE model predicts that the infection will die out eventually. In Regions 2 and 3, the ODE model contains multiple stable equilibriums. Depending on the initial invading bacterial level, multiple disease outcomes may occur. In Region 4, the ODE model has one stable infected equilibrium. It implies that the infection will grow to a high-level eventually.

3.2 *Various disease outcomes with demographic variations in different parameter regions*

In Region 2, the disease stays only if a very high dose of bacterium is inhaled, which is shown in Fig. 1(b) and (c) for $\delta = 0.2 \in [\delta_h, \delta_l]$. The separatrix of different disease outcomes is the unstable equilibrium shown in the dashed blue curves in Fig. 1(a). These dashed blue curves show Mtb concentration increases with the decrease in the δ value. This indicates that a reduction of the bacterial proliferation rate facilitates the disease progression. For comparison, simulations for the SDE model (2.1) with demographic variations demonstrate disease clearance and active disease, as well, which are shown

in Figs 2 and 3. The initial values also determine different disease outcomes. Here, we set the parameter value $\delta = 0.2 \in [\delta_h, \delta_l]$ and fix the other parameter values as in Table 1. Based on 10,000 stochastic realizations of model 2.1, expectations and standard deviations of M_u, M_i, B and T stabilizes by roughly $t = 300$ days. This indicates that solutions of the SDEs (2.1) approach an approximated distribution by time $t = 300$ days. The corresponding simulations in Fig. 2(a) start from $M_u(0) = 5 \times 10^5$, $M_i(0) = 1$, $B(0) = 10$, $T(0) = 1 \times 10^3$. Four stochastic realizations along with one ODE solution are plotted in Fig. 2(b).

At time $t = 300$ days, histograms of approximated stationary distributions for M_u, M_i, B and T are plotted in Fig. 2(c–f). The histogram of the M_u population in Fig. 2(c) fits well with the corresponding normal distribution in the black curve. Moreover, $\mathbb{E}(M_u) = 4.9951 \times 10^5 \approx \bar{M}_{u0}$ in (3.1) implies that the macrophage concentration is at the uninfected level. The histogram of M_i and B are heavily skewed to the right with a peak at zero, which indicates the disease clearance. The histogram of T peaks around $T \approx 20 = \bar{T}_0$ in (3.1) with a long tail. This indicates the T-cell concentration peaks at the uninfected level, with a large variation.

For another set of initial conditions, $M_u(0) = 2 \times 10^4$, $M_i(0) = 1 \times 10^3$, $B(0) = 1 \times 10^5$, $T(0) = 1 \times 10^3$, expectations and standard deviations of M_u, M_i, B and T, based on 10,000 stochastic realizations, stabilize roughly by $t = 100$ days, shown in Fig. 3(a). All four stochastic realizations grow along with the ODE solution, shown in Fig. 3. To end at time $t = 100$ days, histograms of approximated stationary distributions for M_u, M_i, B and T fit well with the corresponding normal distributions shown in Fig. 3(c–f). Moreover, $\mu(M_u) \approx \bar{M}_u(\delta = 0.2)$, $\mu(M_i) \approx \bar{M}_i(\delta = 0.2)$, $\mu(B) \approx \bar{B}(\delta = 0.2)$ and $\mu(T) \approx \bar{T}(\delta = 0.2)$. This indicates an active disease case.

In Region 3, the disease outcome depends on the inhaled dose of bacteria. The disease clearance is shown in the dash-dot curve in Fig. 1(b). The disease progression to LTBI or active TB is shown in the dashed and dotted curves in Fig. 1(c). Simulation results for SDE model (2.1) in Region 3 show similar predictions for the disease clearance and active disease cases in Region 2. We, therefore, omit these two cases in Region 3 and focus on the additional state with low bacterial level generated from the saddle-node bifurcation LP_1. We take parameter value $\delta = 0.27 \in [\delta_l, \delta_m]$ in Region 3. In the ODE model (1.1), the stable low bacterial level equilibrium denoting LTBI is $(\bar{M}_u, \bar{M}_i, \bar{B}, \bar{T}) = (499519.6475, 3.3532, 48.0814, 74.9548)$. Starting at $M_u(0) = 4.99 \times 10^5$, $M_i(0) = 4$, $B(0) = 4$, $T(0) = 75$, based on 10,000 stochastic realizations, expectations and standard deviations of M_u, M_i, B and T stabilize roughly by $t = 300$ days, as shown in Fig. 4(a). Four sample paths and one corresponding ODE solution are graphed in Fig. 4(b). At time $t = 100$ days, approximated stationary distributions for M_u, M_i, B and T have medians as $\text{Median}(M_u) = 4.9893 \times 10^5$, $\text{Median}(M_i) = 3.6589$, $\text{Median}(B) = 52.7568$ and $\text{Median}(T) = 417.5100$. Even though the histograms for M_i, B and T have skewed shapes, the median values for M_u, M_i and B are close to the stable latent infected equilibrium $(\bar{M}_u, \bar{M}_i, \bar{B}, \bar{T}) = (499519.6475, 3.3532, 48.0814, 74.9548)$. Notice that the $\text{Median}(T) = 417.5100$ is much larger than $\bar{T}$. This indicates that the demographic variations significantly affect T-cell population.

In Region 4, the disease will progress to active TB shown in the dash-dot curve in Fig. 1(b) by the ODE model prediction. The nontrivial equilibrium of the ODE model (1.1) at $\delta = 0.35$ is $(\bar{M}_u, \bar{M}_i, \bar{B}, \bar{T}) = (249.9805, 3104.0391, 9.9957 \times 10^7, 1.5145 \times 10^{10})$. Starting at $M_u(0) = 4.99 \times 10^5$, $M_i(0) = 4$, $B(0) = 4$, $T(0) = 75$, based on 100,000 stochastic realizations, expectations and standard deviations of M_u, M_i, B and T stabilize roughly by $t = 1300$ days, as shown in Fig. 5(a). Four sample paths blow up along with the ODE solution shown in Fig. 5(b). At time $t = 1300$ days, the means of approximated stationary distributions for M_i, B and T are close to $\bar{M}_i$, $\bar{B}$ and $\bar{T}$. The mean of M_u is far away from $\bar{M}_u$, but the standard deviation of the approximated stationary distribution is large as well. It implies that small exposure to Mtb bacterial is more likely to develop to active disease.

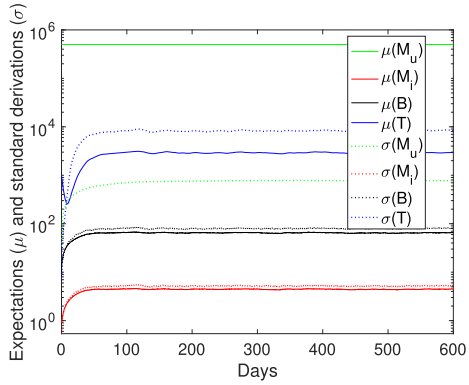

(a) Mean and Std over time.

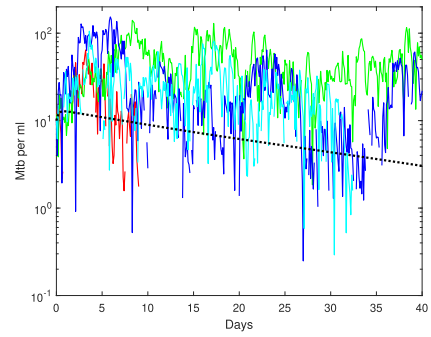

(b) Colored sample paths, black ODE soln.

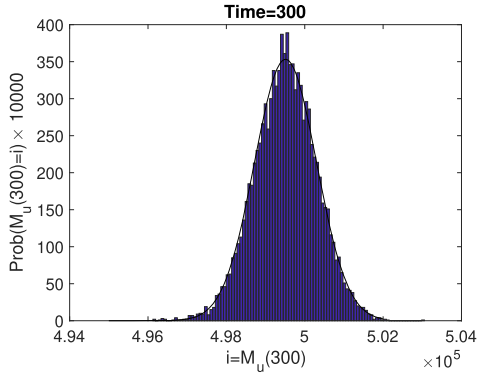

(c) $\mu = 4.9951 \times 10^5$, $\sigma = 790.8575$.

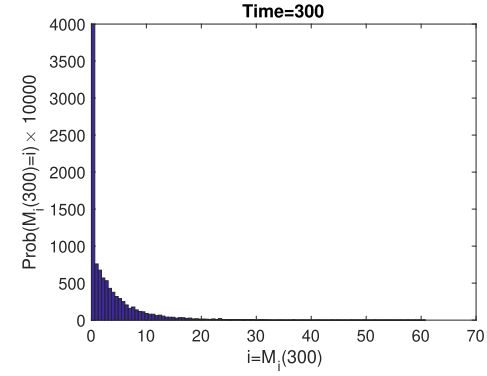

(d) $\mu = 3.2950$, $\sigma = 4.9366$.

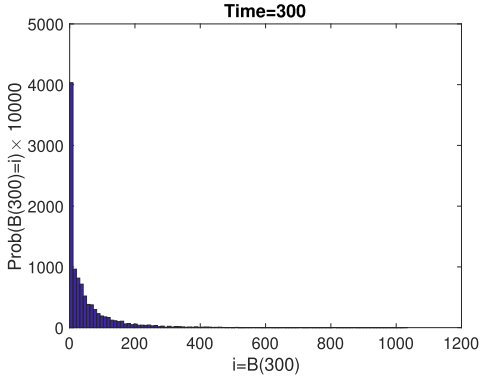

(e) $\mu = 48.6576$, $\sigma = 76.0503$.

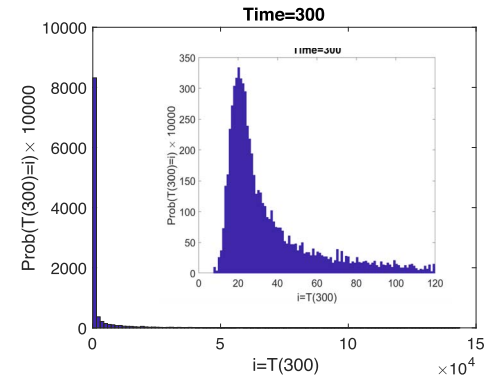

(f) $\mu = 2.2029 \times 10^3$, $\sigma = 7.4485 \times 10^3$.

FIG. 2. Disease clearance or latent TB infection case at $\delta = 0.2$. Mean: μ, standard deviation: σ. (a) Expectations and standard deviations of 10,000 sample paths of the SDE model (2.1). (b) Four stochastic realizations are in coloured curves. Since y-axis is in log scale, the red and cyan curves terminate when they hit the absorption state $B = 0$. The corresponding ODE solution is in the dotted black curve. (c)–(f) Approximate stationary distributions for M_i, M_u, B and T at $t = 300$. 100 bins are used for all four histograms. Initial conditions are $M_u(0) = 4.99 \times 10^5$, $M_i(0) = 1$, $B(0) = 10$ and $T(0) = 1000$. Note that the other parameter values are taken from Table 1.

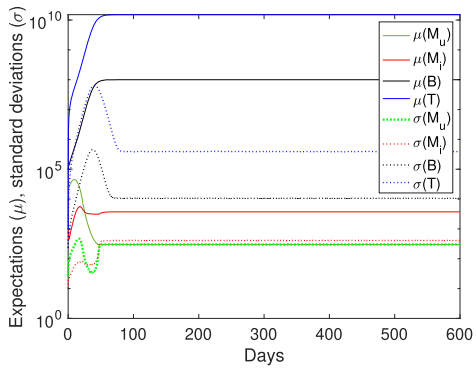

(a) Mean and Std over time.

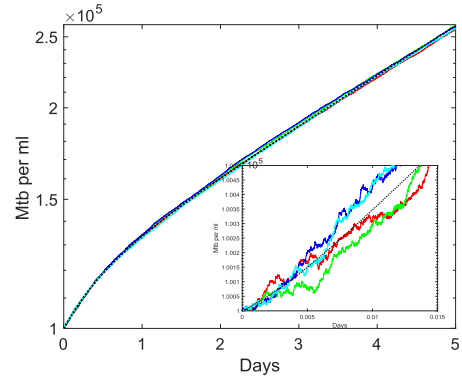

(b) Colored sample paths, black ODE soln.

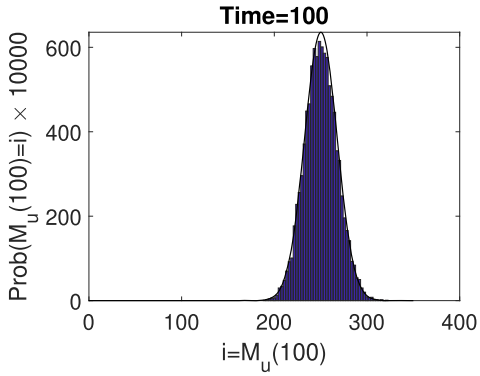

(c) $\mu = 250.2504$, $\sigma = 17.5698$.

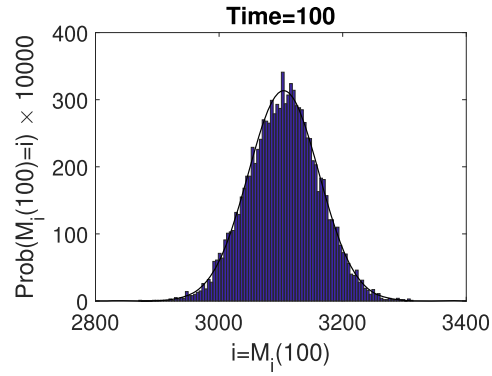

(d) $\mu = 3.1045 \times 10^3$, $\sigma = 57.2839$.

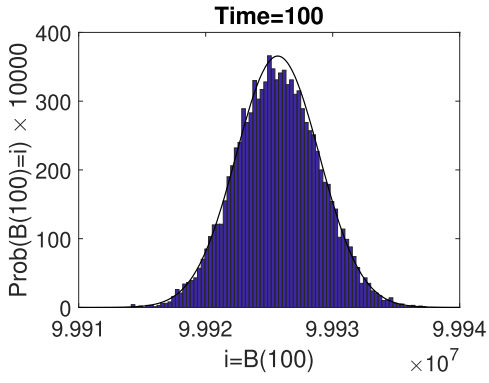

(e) $\mu = 9.9926 \times 10^7$, $\sigma = 3.2734 \times 10^3$.

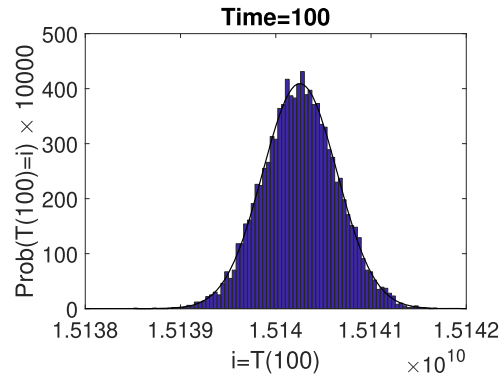

(f) $\mu = 1.5140 \times 10^{10}$, $\sigma = 3.9010 \times 10^5$.

FIG. 3. Active disease case at $\delta = 0.2$. Mean: μ, standard deviation: σ. (a) Expectations and standard deviations of 10,000 sample paths of the SDE model (2.1). (b) Four stochastic realizations in coloured curves vary around the corresponding ODE solution in the dotted black curve. Disease clearance does not occur due to the large number of bacterial load. (c)–(f) Approximate stationary distributions for M_i, M_u, B and T at $t = 100$. 100 bins are used for all four histograms. Initial conditions are $M_u(0) = 2 \times 10^4$, $M_i(0) = 10^3$, $B(0) = 10^5$ and $T(0) = 1000$. Note that the other parameter values are taken from Table 1.

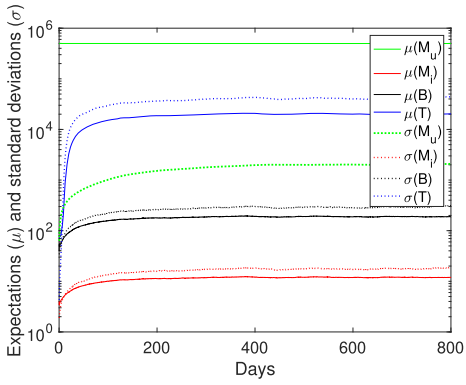

(a) Mean and Std over time.

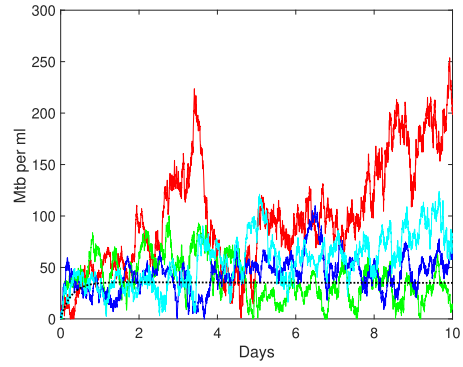

(b) Colored sample paths, black ODE soln.

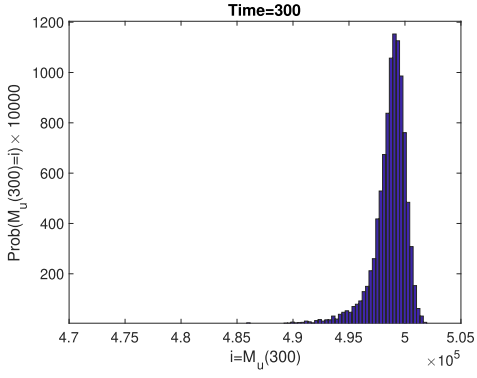

(c) $\mu = 4.9860 \times 10^5$, $\sigma = 1.7721 \times 10^3$.

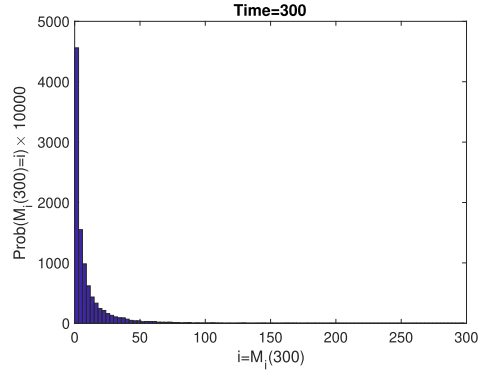

(d) $\mu = 9.2332$, $\sigma = 15.8717$.

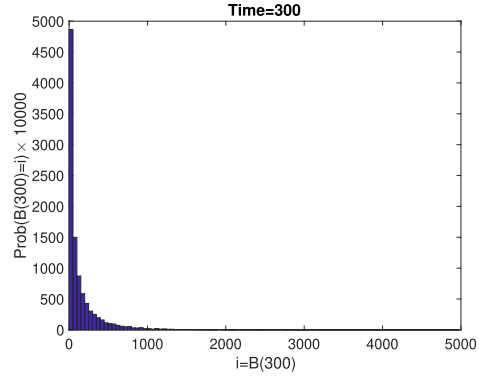

(e) $\mu = 146.4230$, $\sigma = 257.8087$.

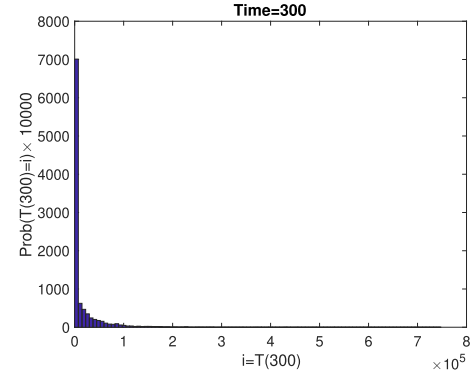

(f) $\mu = 1.5253 \times 10^4$, $\sigma = 3.6356 \times 10^4$.

FIG. 4. Latent infected TB case at $\delta = 0.27$. Mean: μ, standard deviation: σ. (a) Expectations and standard deviations of 10,000 sample paths of the SDE model (2.1). (b) Four stochastic realizations are in coloured curves. The corresponding ODE solution is in the dotted black curve. (c)–(f) Approximate stationary distributions for M_i, M_u, B and T at $t = 300$. 100 bins are used for all four histograms. Initial conditions are $M_u(0) = 4.99 \times 10^5$, $M_i(0) = 4$, $B(0) = 4$ and $T(0) = 75$. Note that the other parameter values are taken from Table 1.

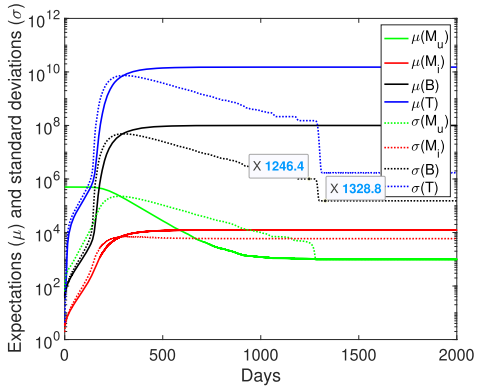

(a) Mean and Std over time.

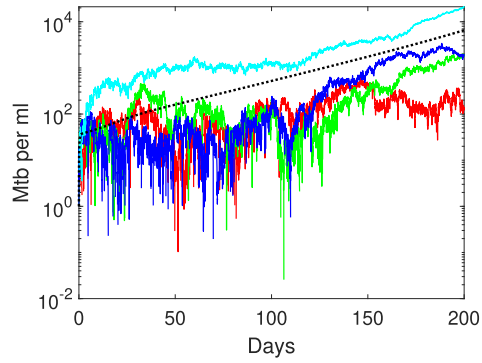

(b) Colored sample paths, black ODE soln.

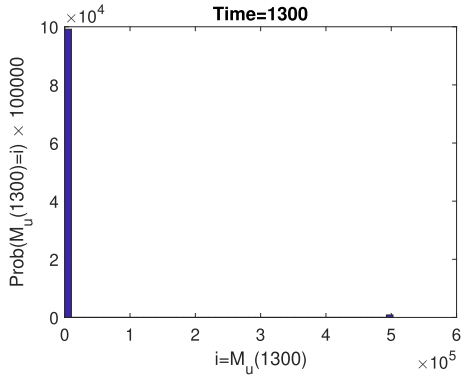

(c) $\mu = 4.4955 \times 10^3$, $\sigma = 4.5856 \times 10^4$.

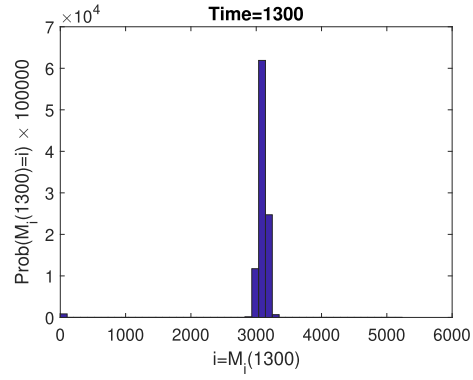

(d) $\mu = 3.0777 \times 10^3$, $\sigma = 290.3366$.

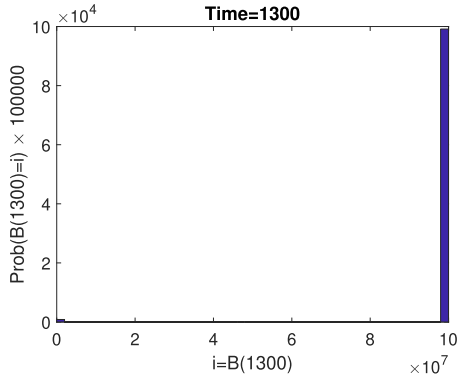

(e) $\mu = 9.9108 \times 10^7$, $\sigma = 9.1779 \times 10^6$.

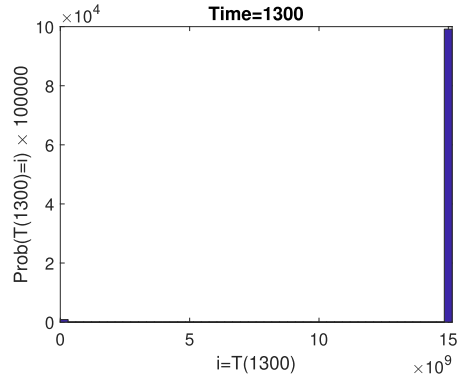

(f) $\mu = 1.5016 \times 10^{10}$, $\sigma = 1.3908 \times 10^9$.

FIG. 5. Active disease case at $\delta = 0.35$. Mean: μ, standard deviation: σ. (a) Expectations and standard deviations of 10,000 sample paths of the SDE model (2.1). (b) Four stochastic realizations are in coloured curves. The corresponding ODE solution is in the dotted black curve. (c)–(f) Approximate stationary distributions for M_i, M_u, B and T at $t = 1300$. 100 bins are used for all four histograms. Initial conditions are $M_u(0) = 4.99 \times 10^5$, $M_i(0) = 4$, $B(0) = 4$ and $T(0) = 75$. Note that the other parameter values are taken from Table 1.

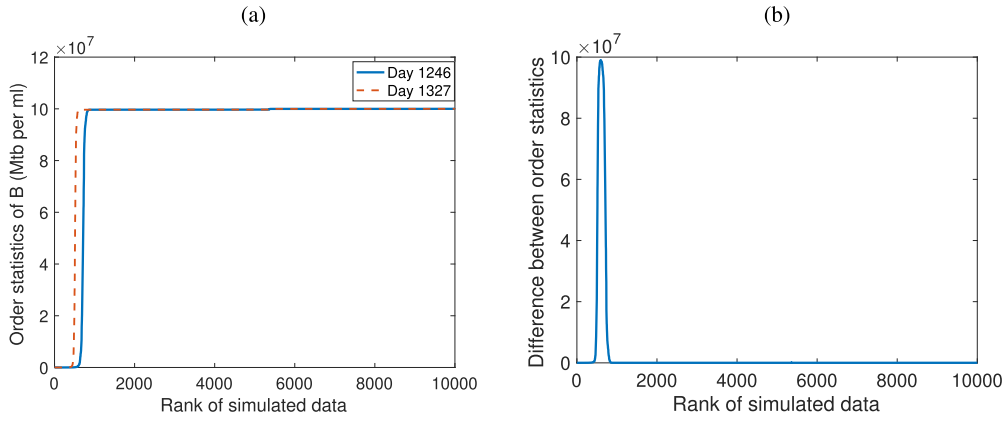

FIG. 6. The horizontal axis denotes the rank of the observations (Mtb concentration B) at Day 1246 and Day 1327. The vertical axis in (a) represents the value of the observation (B value) at each rank. The vertical axis in (b) represents the difference in B value between Day 1246 and Day 1327.

The decreasing parts of the standard deviation curves in Fig. 5(a) indicate that more cell populations converge to their corresponding mean values. Moreover, there are sharp drops at the time roughly between $t \in [1246, 1327]$ in the standard deviation curves of the same figure. The order statistic Fig. 6 suggests that the Mtb concentration, for instance, jumps sharply from a low level to a much higher level. This causes the sharp drop in the standard deviation during the time interval [1246, 1327]. In other words, there are more large values in Day 1327 than in Day 1246. Therefore, the standard deviation is smaller on the later day than the earlier day. It implies that the development of active disease is more likely to happen after Day 250 and before Day 1328. Interestingly, there are some extremely short bars in the histograms in Fig. 5(c–f) that show that there still exists a possibility for disease clearance.

Here are some notes about the SDE simulations in Figs 2– 5.

1. For each figure, we simulate SDE model (2.1) 10, 000 times. With the obtained 10, 000 sample paths, we calculate their expectations and standard deviations at each time step, then demonstrate the trends of convergence in time-series plots shown in the corresponding subfigures (a). Next, we choose simulation times at which the corresponding expectations and standard deviations converge to their stabilized values, i.e. $t = 300$, $t = 100$, $t = 300$, $t = 1300$ for Figs 2– 5, respectively.

2. The bin size for the histogram is chosen as the square root of the number of data points, which is 10, 000 here. The data points are SDE solutions at the simulation end time. Therefore, we choose 100 as the bin size for all four SDE simulations in Figs 2– 5.

3. The baseline parameter values are shown in Table 1. The parameter ranges are provided when variations of parameters are needed. Note that both the baseline values and the ranges of parameters are from existing modelling papers.

4. In Region 2, the ODE model (1.1) contains two stable steady states. We demonstrate disease clearance and active disease under demographic variations in Figs 2 and 3. To generate Figs 2 and 3, we take the same set of parameter values, but different initial conditions (see the figure captions). In Region 3, the ODE model (1.1) has three stable steady states, which represent

disease clearance, LTBI and active disease. SDE simulations for disease clearance and active disease show the similar behaviour as in Figs 2 and 3. We, therefore, omit the graphs for these two cases, but only demonstrate the LTBI case in Fig. 4. In Region 4, the ODE model (1.1) has only one steady state, which represents active disease. Interestingly, the SDE simulation predicts a possibility for the occurrence of disease clearance (see the tiny bars in histograms in Fig. 5). Moreover, the curves representing standard derivations in Fig. 5 have decreasing parts with sharp drops. These drops imply that the development of active disease is more likely to happen from the end of the first year to the third year after the initial exposure.

4. Influences of Bacterial and Host Factors on Disease Progression Speed and Combination Therapy Outcomes

In this section, we consider the impact of both the bacterial factor (i.e. the infected macrophage proliferation rate δ) and host factors (including the infected macrophage loss rate b, the cell-mediated immunity rate γ and macrophages' bacteria killing rate η) in evaluating the pathogen-directed (antibiotic) therapy with adjunctive HDTs. Previous work Zhang *et al.* (2021) suggests that these four parameters have the most statistically significant impacts on model behaviours. We first study the disease dynamics influenced by both the bacterial proliferation rate modulated by pathogen-directed therapy and the host immune components (b, γ and η) altered by HDT. Our results suggest that host immune responses can both promote and hinder disease progression. Different disease outcomes depend on the relation between the numbers of Mtb engulfed by and released by macrophages. Considering the stochastic variations from both the cell populations and the adherence to therapies, we investigate the SDE model (2.2) with both demographic and environmental variations to provide insight into the pathogen- and host-directed combination therapy developments. Next, we derive a quadratic relationship between the Mtb spreading speed and the bacterial proliferation rate δ. Then, we further investigate the disease progression speed under the influences of both pathogen-directed therapy (such as antibiotics affecting δ) and HDT (such as vitamin D affecting b, γ and η). Our results demonstrate the advantages of the combination therapy.

4.1 *Bacterial concentration affected by both the bacterial proliferation rate and acquired defects*

The analysis results from the ODE model (1.1) in Fig. 1 indicate the possibility of disease clearance if the bacterial proliferation rate δ falls in Region 2, the potential to progress to LTBI or active TB if δ is in Region 3, and a progression to active TB if δ is in Region 4 by the ODE model prediction. There also exist δ values, which guarantee disease clearance. However, this δ value window is slim and demonstrated in yellow strips in Fig. 7. We denote this parameter region for disease clearance as Region 1. The four parameter regions are delimited by saddle node (LP) and transcritical (BP) bifurcations. Two parameter bifurcation analyses were carried out via Matcont (Fabri *et al.*, 2011). The corresponding bifurcation diagrams are plotted in Fig. 7 and illustrate the four regions associated with bacterial proliferation rate δ and three parameters denoting host immune responses (i.e. b, γ and η). It is shown that an increase in the loss rate of infected macrophages b and a decrease of both the cell-mediated immunity rate γ and the bacteria killing rate by macrophages η impede disease clearance (in Region 1 and 2) and facilitate the disease development (in Regions 3 and 4). Note that parameter relations $N_1 > N_3$ and $N_2 > N_3$ are taken for the bifurcation analysis under the assumption that macrophages are infected with virulent Mtb and undergo necrosis The Editors of Encyclopaedia Britannica (2022). The bifurcation parameter ranges are provided by Gammack *et al.* (2005): $\delta \in (0, 0.35)$, $b \in (0.05, 0.5)$,

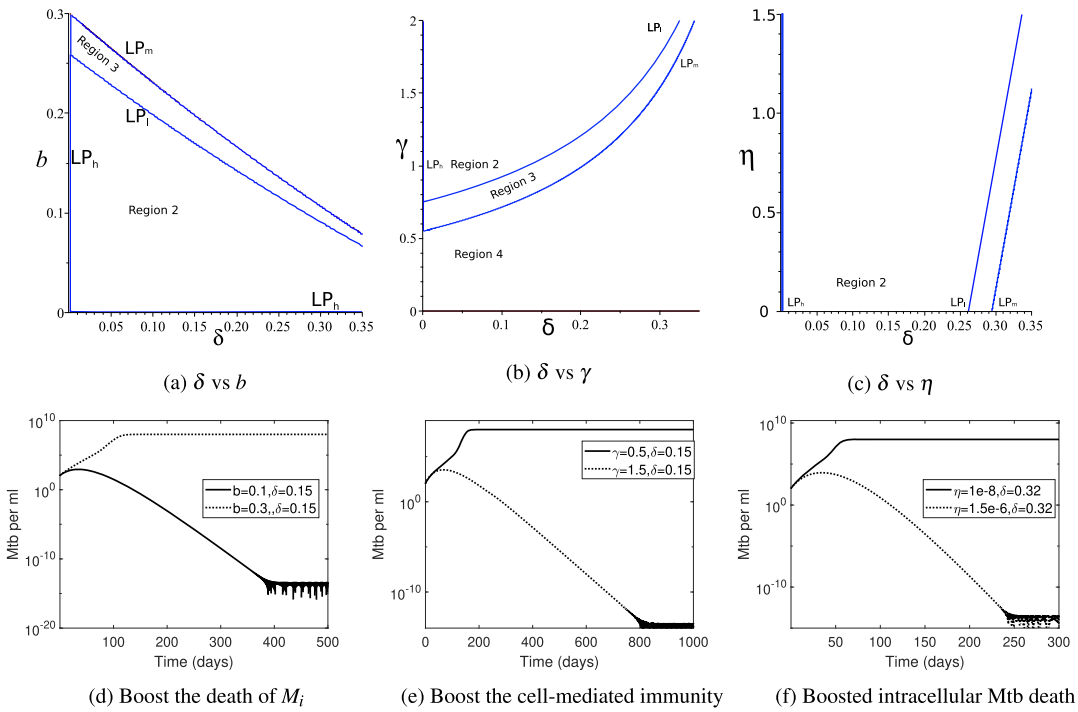

(a) δ vs b (b) δ vs γ (c) δ vs η

(d) Boost the death of M_i (e) Boost the cell-mediated immunity (f) Boosted intracellular Mtb death

FIG. 7. The influence of host immune response to bactericidal drug therapy. (a), (b) and (c) are two-parameter bifurcation diagrams. Blue and red curves denote saddle node (LP) and transcritical (BP) bifurcations, respectively. Numerical simulation (d) corresponds bifurcation diagram (a), (e) corresponds (b) and (f) corresponds (c). (d) shows that an increase in the death of infected macrophages (b) favours Mtb infection. While (e) and (f) shows that boosting the cell-mediated immunity (γ) and the intracellular Mtb death rate (η) benefit the host defence. Note that we take the other parameter values from Table 1 and initial values as $M_u(0) = 10$, $M_i(0) = 1$, $B(0) = 100$ and $T(0) = 1000$.

$\gamma \in (0.1, 2)$ and $\eta \in (1.25 \times 10^{-9}, 1.25 \times 10^{-7})$. Other than the bifurcation parameters, the other parameter values are taken from Table 1.

HDTs can modulate host immunity, which in turn tune the associated parameter values. However, these parameter values are influenced by environmental variations due to the patient system's natural regulation and the stability of adjunct drug concentrations. We then use the second SED model (2.2) that considers both demographic and environmental variations to evaluate the Mtb concentration. The mean values δ_s, b_s, γ_s and η_s are taken as the values of δ, b, γ and η in Table 1. We take a return rate relation as $\alpha_i = 2\sigma_i^2$ for $i = 1, ..., 4$ to avoid a large variability during the therapy. Fast and slow return rates are taken as $\alpha_i = 0.5$ and $\alpha_i = 0.05$ for simulations of SEDs (2.2). For the case that the pathogen-directed and host-directed therapy combination affects the loss rate of infected macrophages b and the bacterial proliferation rate δ, disease outcomes are predicted by bifurcation analyses of the ODE model (1.1) in Fig. 7(a), and by the second SDE model (2.2) in Fig. 8. In Region 2, none of the four Mtb sample paths eventually blow up for the fast return rate, but two of them develop to high Mtb level if the return rate is slow. In Region 3, all four Mtb sample paths blows up. But the sample paths take off slower for the fast return rate than the slow return rate. We do not consider Region 4. Because TB will definitely develop to active disease in this region, we expect therapies will bring parameters away from Region 4. For the

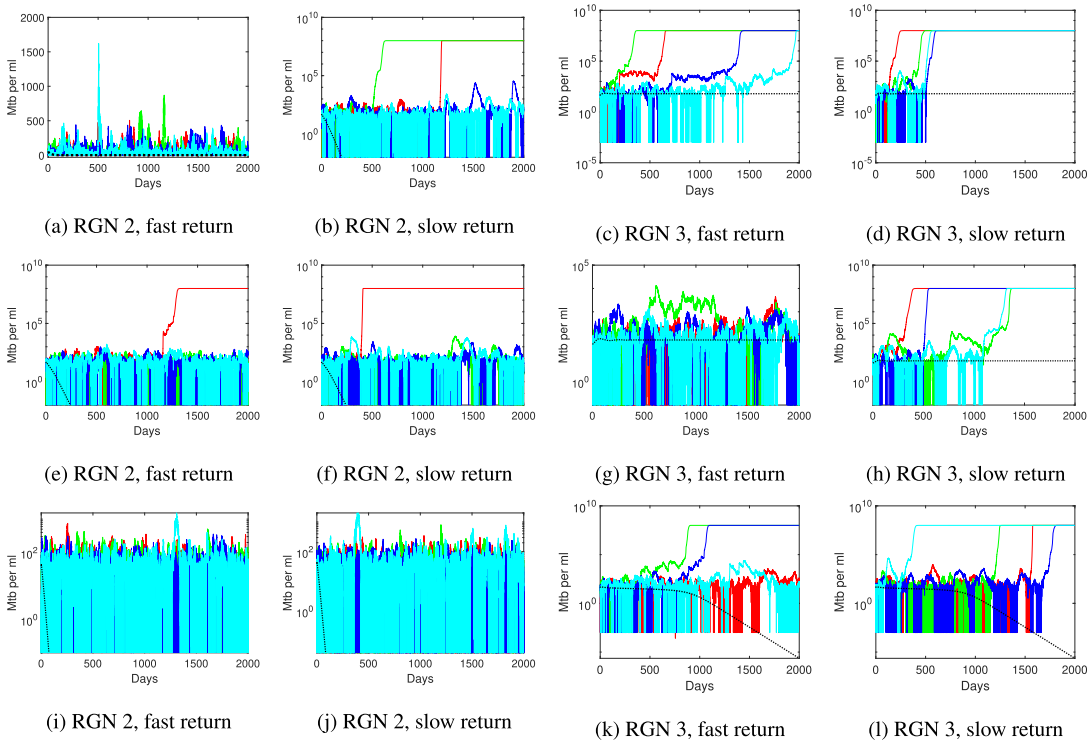

(a) RGN 2, fast return (b) RGN 2, slow return (c) RGN 3, fast return (d) RGN 3, slow return

(e) RGN 2, fast return (f) RGN 2, slow return (g) RGN 3, fast return (h) RGN 3, slow return

(i) RGN 2, fast return (j) RGN 2, slow return (k) RGN 3, fast return (l) RGN 3, slow return

FIG. 8. Four sample paths for SDEs (2.2) with demographic and environmental variations is in coloured curves. Fast return rate is $\alpha_i = 0.5$, slow return rate is $\alpha_i = 0.05$ and the return rate satisfies $\alpha_i = 2\sigma_i^2$. The ODE solution for model (1.1) is in black curve. Parameter values are (1) (in the first row) $\delta = 0.2$, $b = 0.1$ (Region 2) and $b = 0.17$ (Region 3), (2) (in the second row) $\delta = 0.2$, $\gamma = 1.5$ (Region 2) and $\gamma = 1.05$ (Region 3) and (3) (in the third row) $\eta = 0.5 \times 10^{-7}$, $\delta = 0.1$ (Region 2) and $\delta = 0.285$ (Region 3). The other parameter values are from Table 1.

therapies targeting parameters γ and δ combination and η and δ combination, Fig. 8 indicate similar results. Our results suggest that a pathogen-directed and host-directed therapy combination can bring parameter values to Region 2 with a fast return rate (i.e. drug concentration can quickly converge to the desired level). As a result, the patient can spend more time in the disease clearance or latent infection status. This indicates this therapy combination slows down disease progression.

4.2 *A positive relationship between the bacterial proliferation and the slope of disease progression*

Figure 9 shows that the bacterial proliferation rate has a positive relationship with the slope of disease clearance and progression after exposure. More precisely, the slope of bacterium concentration is determined by the dominant eigenvalue. Its linear approximation is a quadratic function of the bacterial proliferation rate δ. The following derivation is inspired by methods used by Rosenberger *et al.* (2004) and Yu (2005).

TB infection starts from the inhalation of droplet nuclei carrying Mtb by a healthy individual. The small amount of inhaled tubercle bacilli can be treated as a small positive perturbation of the trivial steady state $(\bar{M}_{u0}, \bar{M}_{i0}, \bar{B}_0, \bar{T}_0)$. The local stable trivial steady state represents the possible scenario

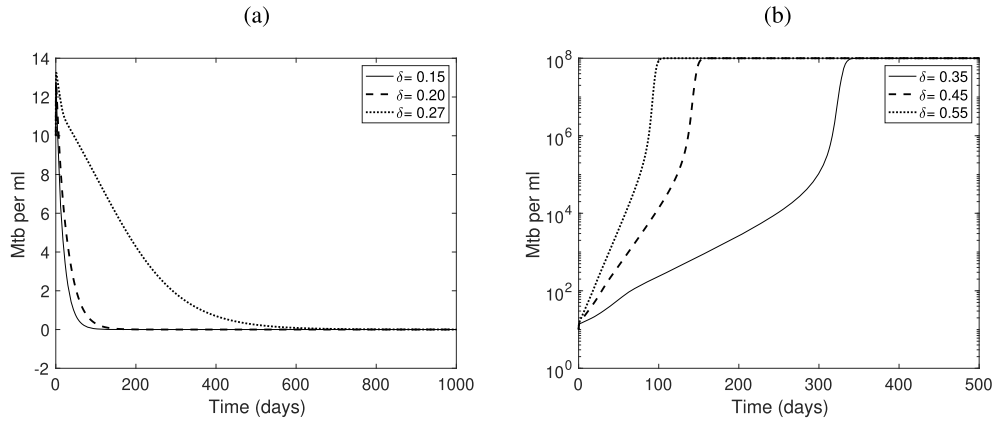

FIG. 9. Predicted bacteria concentration decay and growth for a case that a healthy individual ($M_u(0) = \bar{M}_u = 500,000\,cells/ml$ and $T(0) = \bar{T} = 1000\,cells/ml$) inhales infectious droplet nuclei carrying small amount of Mtb pathogens ($M_i(0) = 1\,cells/ml$ and $B(0) = 10\,cells/ml$). The threshold bacterium growth rate is $\delta_0 = 0.2956/B/day$. $\delta < \delta_0$ results early clearance. $\delta > \delta_0$ causes disease progression. The slope of the Mtb time history is positive, related to the bacterium growth rate δ. The other parameter values are taken from Table 1.

of bacterial clearance, while the unstable trivial steady state means insufficient immune responses fail to clear the infecting bacteria, and thus disease starts to progress. Figure 9 shows that the rate of early clearance and disease progression depends on the bacterial proliferation rate δ. A higher bacterial proliferation rate results in a slower bacterial decline and a faster disease progress. It also suggests the existence of a threshold value of the bacterial proliferation rate δ, which separates the early clearance and disease progression in early infection.

Mathematically, the slope of bacteria decline and progression is dependent on the largest eigenvalue of the model (1.1) at the trivial steady state ($\bar{M}_{u0}$, $\bar{M}_{i0}$, $\bar{B}_0$, $\bar{T}_0$). Consider a general system $\dot{u} = f(u, \mu)$, where $u \in \mathbb{R}^n$, $\mu \in \mathbb{R}^m$ and $f \in \mathbb{R}^{n\times m}$ denote state variables, parameters and a vector of n functions. Suppose that $u_e = u_e(\mu)$ represents the trivial steady state, i.e. $f(u_e(\mu), \mu) = 0$. The small amount of invading Mtb pathogens is modelled as a small positive perturbation nearby the trivial steady state, i.e. $x = u - u_e \in \mathbb{R}^n$. The growth of the perturbation indicates the development of the infection, while a decay of x corresponds to the disease clearance. The evolution of disease progression is governed by the perturbation of the equation as follows:

$$\dot{x} = \dot{u} - \dot{u}_e = f(x + u_e(\mu), \mu) = f(u_e(\mu), \mu) + x \left[\frac{\partial f_i(u_e(\mu), \mu)}{\partial x_j}\right]_{n\times n} + \text{ higher order terms.}$$

If the preceding system is hyperbolic, i.e. all eigenvalues of $A = \left[\partial f_i(u_e(\mu), \mu)/\partial x_j\right]_{n\times n}$ have nonzero real parts, then the system can be approximated by the linear system $\dot{x} = A\,x$. Further, we assume A has n distinct eigenvalues λ_i with associated eigenvector v_i, i.e. $(A - \lambda_i I)v_i = 0$ for $i = 1, \ldots, n$. We form a matrix $T = (v_1, v_2, \ldots, v_n)$ and have $A = T\Lambda T^{-1}$. Then the general solution of the linearized system $\dot{x} = A\,x$ with a chosen initial condition $x_0 \in \mathbb{R}^n$ is a linear combination of $v_1 e^{\lambda_1 t}$, $v_2 e^{\lambda_2 t}$, $\ldots$, $v_n e^{\lambda_n t}$. That is, $x(t) = e^{At}x_0 = Te^{\lambda t}T^{-1}x_0 = (v_1 e^{\lambda_1 t}, v_2 e^{\lambda_2 t}, \ldots, v_n e^{\lambda_n t})T^{-1}x_0$. Assuming λ_1 is the dominant eigenvalue (the spectral radius of the matrix A), i.e. $\lambda_1 = \rho(A) = \max\{\lambda_i, i = 1, \ldots, n\}$, then $e^{\lambda_1 t}$ is

the most influential component in the solution basis set of $x(t)$. The evolution of the perturbation $x(t)$ is the change of the original variable $u(t)$. It is determined by the dominant eigenvalue λ_1. Moreover, if $\lambda_1 < 0$, the perturbation dies out ($x(t) \to 0$). The infecting bacteria are eliminated by host immune responses. If $\lambda_1 > 0$, the perturbation grows and the infection develops. The threshold for the infection clearance and establishment is $\lambda_1 = 0$ and $\lambda_i < 0$ for $i = 2, \ldots, n$.

Taking the general system $\dot{u} = f(u, \mu)$ as the model (1.1) and its trivial equilibrium as $u_e = (\bar{M}_{u0}, \bar{M}_{i0}, \bar{B}_0, \bar{T}_0)$. The corresponding eigenvalues are roots of the following characteristic polynomial:

$$\begin{aligned} P(\lambda) &= (\lambda + \mu_T)(\lambda + \mu_M)(\lambda^2 + c_1\lambda + c_2) = 0, \quad \text{where} \\ c_1 &= (b + \gamma) + \frac{s_M}{\mu_M}(N_3\beta + \eta) - \delta \quad \text{and} \\ c_2 &= \left\{ \eta\frac{s_M}{\mu_M} - \beta\left[(N2 - N3)\frac{\gamma}{b+\gamma} + (N1 - N3)\frac{b}{b+\gamma} \right]\frac{s_M}{\mu_M} - \delta \right\}(b + \gamma). \end{aligned} \tag{4.1}$$

That is,

$$\lambda_1 = -\frac{c_1}{2} + \frac{c_1}{2}\sqrt{1 - \frac{4c_2}{c_1}},\ \lambda_2 = -\frac{c_1}{2} - \frac{c_1}{2}\sqrt{1 - \frac{4c_2}{c_1}},\ \lambda_3 = -\mu_T,\ \lambda_4 = -\mu_M, \tag{4.2}$$

where $\lambda_{3,4} < 0$ due to the positiveness of all parameter values. The expression of the preceding equation for $P(\lambda) = 0$ and $\bar{M}_{u0} = s_M/\mu_M$ Zhang *et al.* (2020) determine the local stability of the trivial equilibrium.

Here, we use the eigenvalues associated with the trivial equilibrium to further investigate the disease progression speed. Extracellular bacteria are introduced into the system by three main ways, extracellular bacterial proliferation, bacterium release by the programmed cell death of infected macrophages and bacterium release from infected macrophages killed by T-cell-mediated immune responses. In early infection, we assume the loss of extracellular Mtb pathogens is caused only by macrophage phagocytosis. We omit the loss of infected macrophages by T-cell-mediated immune responses. The per capita rate of macrophage phagocytosis is $N_3\beta + \eta$ per uninfected macrophage per bacterium. Considering the (asymptotic) upper bound of the uninfected macrophage $\bar{M}_{u0} = s_M/\mu_M$, the maximum bacterial loss rate is $(N_3\beta + \eta)\bar{M}_{u0} = (N_3\beta + \eta)s_M/\mu_M$ per bacterium, which is assumed to be greater than the bacterium proliferation rate δ. Further, assuming that all invading pathogens are phagocytized, i.e. $\delta < (N_3\beta+\eta)s_M/\mu_M$. This implies $\delta < b+\gamma+(N_3\beta+\eta)s_M/\mu_M$, which is equivalent to $c_1 > 0$. Therefore, if $c_2 < 0$, the square root $\sqrt{1 - \frac{4c_2}{c_1}}$ is greater than one, then λ_1 and λ_2 are real numbers and have opposite signs. If $c_2 > 0$, then the real parts of λ_1 and λ_2 are all negative.

If $c_2 = 0$, a zero-eigenvalue bifurcation occurs at $\lambda_1 = 0$, at which

$$\delta = \delta_0 \triangleq \eta\frac{s_M}{\mu_M} - (N2 - N3)\frac{\gamma}{b+\gamma}\beta\frac{s_M}{\mu_M} - (N1 - N3)\frac{b}{b+\gamma}\beta\frac{s_M}{\mu_M}. \tag{4.3}$$

The number of 'next generation' infectious Mtb bacteria produced by a single infectious bacterium introduced near the trivial equilibrium is (1) at most δ by cell proliferation, or (2) $(N_1 - N_3)$ and $(N_2 - N_3)$ by the death of infected macrophages and T-cell-mediated immune response with the probability of $b/(b + \gamma)$ and $\gamma/(b + \gamma)$, respectively. In the meantime, phagocytosis can kill at most η engulfed

bacteria. We assume the uninfected macrophages is at the maximum available level s_M/μ_M. Therefore, the infection dies out if $\delta < \delta_0$ (i.e. $c_2 > 0$) but stays if $\delta > \delta_0$ (i.e. $c_2 < 0$, $\lambda_1 > 0$, $\lambda_2 < 0$). The threshold is $\delta = \delta_0$. Considering the parameter values in Table 1, the bifurcation analysis shown in Fig. 1(a) shows that the δ parameter range for latent infected TB (roughly 80% of the total TB infected individuals) is [0.2621, 0.2944], which is very close to $\delta_0 = 0.2957$. That is, for $\delta \in [0.2621, 0.2944]$, $|\delta - \delta_0| \ll 1$ (then $|c_2| \ll 1$), we thus expand the square root in λ_1 in Equation (4.2) at $\delta = \delta_0$. This yields

$$\begin{aligned}\sqrt{1-\frac{4c_2(\delta)}{c_1(\delta)}} &= 1 - 2\,\frac{1}{c_1(\delta_0)}\,[-(b+\gamma)]\,(\delta-\delta_0) + \cdots, \quad \text{thus}\\ \lambda_1 &= -\frac{c_1(\delta)}{2} + \frac{c_1(\delta)}{2}\left\{1 - 2\,\frac{1}{c_1(\delta_0)}\,[-(b+\gamma)]\,(\delta-\delta_0) + \cdots\right\}, \qquad (4.4)\\ &\approx (b+\gamma)\,\frac{c_1(\delta)}{c_1(\delta_0)}\,\big(\delta-\delta_0\big) = -\frac{c_1(\delta)c_2(\delta)}{c_1(\delta_0)}.\end{aligned}$$

Based on the feasible parameter ranges, $c_1 > 0$ holds. We approximate the dominant eigenvalue λ_1 as a quadratic function of the bacterial proliferation rate δ. We notice that the dominant eigenvalues determines the changing slope of the bacteria concentration. This implies that if $\delta < \delta_0$ (or $\delta > \delta_0$), the Mtb bacterial concentration declines (or grows) in a speed with a quadratic relationship of the bacterial proliferation rate δ. This speed is slowing down if δ is approaching to its critical value δ_0 from both sides but is speeding up if δ is moving away from δ_0. This is demonstrated by numerical simulations in Fig. 9.

4.3 *Using vitamin D as an adjunctive therapy*

Vitamin D has been shown to promote macrophage maturation, which in turn inhibits the intracellular Mtb growth and enhance antimicrobial immune response (Behar *et al.*, 2011; Du *et al.*, 2017; Hasegawa *et al.*, 2009; Schwander *et al.*, 1998). A dose-dependent vitamin D induced reduction in Mtb growth can reach 75.7% (Meermeier & Lewinsohn, 2018). The strengthened antimicrobial immune response can be described as an enhanced bacteria killing rate by macrophages, η. Equations (4.1) and (4.4) indicate that the dominant eigenvalue λ_1 has a negative quadratic relationship with η. We experiment with different parameter values for η and δ to demonstrate the effect of vitamin D therapy and the combination therapy of antibiotic and vitamin D. We adopt the parameter ranges for $\delta \in (0, 0.35)$ and $\eta \in (1.25 \times 10^{-9}, 1.25 \times 10^{-7})$ (Gammack *et al.*, 2005). The simulation in Fig. 10(a) shows that the bacterial decrease slope is much steeper for the solid curve than the dashed one. This supports the idea of using vitamin D as an adjunct therapy for enhanced immune response and obtaining a favourable disease outcome. Figure 10(b) demonstrates that the dotted curve with a reduced value of δ shows a faster decay rate. This confirms the promising therapy outcomes of adding vitamin D to modulate the host immune response alongside the antibiotic therapy (Tobin, 2015).

Moreover, vitamin D has been suggested to play a pivotal role on interferon-γ (IFN-γ)-induced antimicrobial pathway in macrophages against Mtb infection (Gombart, 2009). In vitamin D-sufficient sera, IFN-γ promotes the production of antimicrobial peptides such as Cathelicidin by macrophages (Marino & Kirschner, 2004). It in turn enhances the antimicrobial activity by lowing the intracellular survival (Wheelwright *et al.*, 2014). Reducing intracellular Mtb survival induces a reduced level of bacterial release in T-cell-mediated cell death. That means a decrease on the values of N_2, which denotes average numbers of bacteria released by T-cell-induced death of infected macrophage. It is also reported

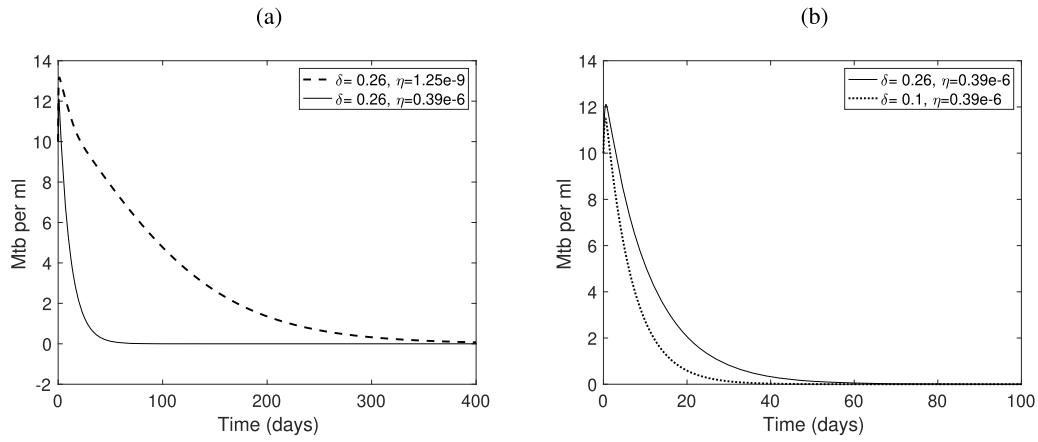

FIG. 10. Bacterial clearance (a) at macrophages killing rate η with (solid) and without (dashed) vitamin D boost, and (b) with only vitamin D boost (solid) and with both vitamin D and antibiotic therapies (dotted). Initial conditions are taken for a case that a healthy individual ($M_u(0) = \bar{M}_u = 500000\,cells/ml$ and $T(0) = \bar{T} = 1000\,cells/ml$) inhales infectious droplet nuclei carrying small amount of Mtb pathogens ($M_i(0) = 1\,cells/ml$ and $B(0) = 10\,cells/ml$). The other parameter values are taken from Table 1.

that vitamin D promotes infected cell apoptosis (Cohen *et al.*, 2019), which induces a decrease on the values of both N_1 and b. Note that N_3 denotes the average number of bacteria phagocytized by an uninfected macrophage. The parameter ranges for N_1, N_2 and N_3 from Gammack *et al.* (2005) are $N_1 \in (50, 100)$, $N_2 \in (20, 30)$ and $N_3 \in (25, 50)$. The loss of infected macrophages caused by cell death and cell-mediated killing are at the rates of b and γ. The same paper also provides the parameter ranges for $b \in (0.05, 0.5)$ and $\gamma \in (0.1, 2)$. If $N_1 > N_3$ and $N_2 > N_3$, the simulation in Fig. 11(a) shows a positive relation of between the dominant eigenvalue λ_1 and the parameters b and γ. The positive value of λ_1 represents the positive slope of the disease progression. In this case, a large number of intracellular Mtb are released from the death of infected macrophages. It results that an increase in cell death and cell-mediated killing benefits Mtb invasion. In the case that a small number of intracellular Mtb are released from the death of infected macrophages, we assume that $N_1 < N_3$ and $N_2 < N_3$.

The simulation in Fig. 11(b) shows that λ_1 is negatively related with the parameters b and γ. The negative slope indicates disease clearance. In this case, most of the intracellular Mtb are killed, and thus the disease is then under control. Moreover, the magnitude of λ_1 is positively related to the infected macrophage loss/bursting rate b and cell-mediated immunity rate γ. This indicates that the stronger the immune responses, the faster the infection is eliminated. Therefore, immune responses hinder the progression of the infection and benefit the host in this case. To reduce the intracellular Mtb load, vitamin D supplementation has been suggested as a host-directed adjunctive therapy (Tobin, 2015). Vitamin D can help to inhibit intracellular bacterial growth through antimicrobial mechanisms (Meermeier & Lewinsohn, 2018), which modulates the immune response to benefit the host defence against the Mtb infection.

5. Conclusion and Discussion

Despite the recent advancement of antibiotic TB drugs, antimicrobial resistance and strict medication adherence are still important issues for achieving effective therapeutic outcomes. As a result, HDT is proposed as an adjunctive therapy to modulate the host immune response against the Mtb pathogen.

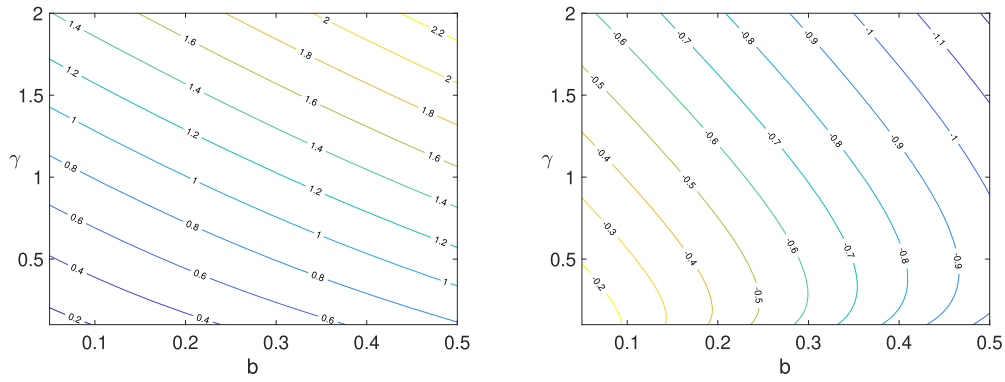

(a) $N_1 > N_3$ and $N_2 > N_3$ (b) $N_1 < N_3$ and $N_2 < N_3$

FIG. 11. Contour plots of the dominant eigenvalue λ_1 as a function of b and γ. The parameter values for N_1, N_2 and N_3 used in simulations are (a) $N_1 = 50$, $N_2 = 30$, and $N_3 = 25$, (b) $N_1 = 10$, $N_2 = 20$ and $N_3 = 25$. The other parameter values are taken from Table 1.

As an emerging and promising approach for attaching the intractable TB disease, a comprehensive understanding of the Mtb-host dynamics is needed to develop treatments that combine pathogen- and HDTs.

In this paper, we focused on the factors that can be modulated by pathogen- and host-directed therapies to explore the various disease outcomes. Being the mainly affected parameter of pathogen-directed therapy, bacterial proliferation rate is shown to have a positive relationship with the disease progression. However, the infected macrophage death rate b and cell-mediated immunity rate γ can both benefit and impede the infection, which depends on the relation between the number of bacteria engulfed and released by macrophages; see Fig. 11. If macrophages engulf more Mtb bacteria than they release, host immune responses benefit the disease control. Otherwise, host immune responses benefit the pathogen development.

There is another example that immune responses lead to both unfavourable and favourable consequences. Increasing the loss of the infected macrophages can cause active disease, which is shown in Fig. 7(d). However, increasing the macrophage- and T-cell-mediated immune responses benefit the clearance of disease, which is shown in Fig. 7(e) and (f).

The different disease outcomes can be represented as trivial, multiple and nontrivial steady states in a deterministic ODE model. The disease progression between latent TB infection to active disease is a transition between co-existing multiple steady states and single nontrivial steady state. The transition critical point is a saddle-node bifurcation. Analogously, the fate of the disease after initial exposure is determined by a transcritical bifurcation. Therefore, transcritical and saddle-node bifurcations serve as separatrices in the parameter space. Focusing on the therapy targeting parameters, including the bacterial proliferation rate δ, the infected macrophage loss rate b, the cell-mediated immunity rate γ and the macrophage killing rate η, 1D and 2D bifurcation analyses delimit the parameter range for different disease outcomes. We then use the identified parameter regions and consider the demographic variations in Mtb pathogen and host immune cell populations and the environmental variations on host immunity under therapies to study the disease dynamics.

We developed two Itô stochastic models with only demographic variations and with both demographic and environmental variations were developed based on the deterministic in-host TB model. In

Region 2, the ODE model (1.1) predicts that the TB infection can be eliminated if the initial condition is a low infection level or can progress to active disease if the initial condition is a high infection level. With a low initial infection level, indicating initial exposure to Mtb pathogens, the SDE model (2.1) with demographic variations predicts that the expectation of the uninfected macrophages' population is close to the uninfected macrophage population from the deterministic model. The histogram of the approximate stationary distribution of the uninfected macrophage population is close to a normal distribution. Even though infected macrophages and bacterial populations have nonzero but small expectations, their peaks are close to zero. Therefore, after initial exposure, the SDE model (2.1) predicts that uninfected and infected macrophage and Mtb bacterial populations have a low level of variation due to demographic variations in cellular level. Interestingly, the stationary distribution of the T-cell population peaks at the uninfected level from the deterministic model prediction, but its mean is relatively large and has a large standard deviation. This large variation implies large stochastic variations applied on T-cell population; see Fig. 2.

If initial conditions take high-level infection values, the histograms of approximate stationary distribution for immune cell and bacterial populations are close to normal distribution shapes. Moreover, their means are close to the deterministic model prediction. However, the Mtb bacterial and T-cell populations have large standard deviations, which implies that the stochastic demographic fluctuations have large influences on those two populations, as seen in Fig. 3. In Region 3, with low initial infection level, the SDE model prediction shows similar patterns as the prediction in Region 2, as seen in Fig. 4. In Region 4, where the disease will eventually develop to active disease according to the deterministic model prediction, the expectations of the SDE model prediction agree with the deterministic model prediction. However, the standard deviation of uninfected macrophage, Mtb bacterial and T-cell populations are large. This implies large stochastic fluctuations in the cellular level, as shown in Fig. 8. Interestingly, there exist small bars in Fig. 8(c–f) that are close to the uninfected equilibrium of the deterministic model prediction. These small bars imply a small possibility of disease clearance.

In addition to demographic variations, the SDE model (2.2) considers environmental variations from therapies. The pathogen-directed therapy mostly influence the pathogen proliferation rate δ. The HDT mainly affects the host-immunity parameters (b, γ and η). The simulation results imply that a fast return rate, along with host-immunity parameters taken in clearance region of Region 2, are most likely to control the disease progression. Note that the return rate indicates the speed of returning to the desirable therapy outcome by drug administration; see Section 2.2.

The basic reproduction number in the parameter Region 4 is greater than one, but the approximated stationary distribution results in Fig. 8(c–f) show the possibility of disease clearance. This probability can be studied through continuous-time Markov chain model. This will be the topic for a future project.

Note that the coarse-graining model (1.1), which we used in this study, is based on the computational models constructed by Wigginton & Kirschner (2001). A feature of the model (1.1) is that it only includes the essential cell populations and biological mechanisms for the Mtb infection but demonstrates various disease outcomes. This implies that the model (1.1) with a smaller number of variables and parameters can still predict the complex disease dynamics. This feature allows for a rigourous mathematical analysis, which leads to robust qualitative results over large parameter ranges. The simple structure of this model also reveals the underlying causal mechanisms for model behaviours (Zhang *et al.*, 2014). The baseline parameter values in Table 1 are inherited from the computational model by Wigginton & Kirschner (2001). The parameters, which can be varied by therapies, are provided with their ranges from multiple studies. The absence of parameter estimation from experimental data does not weaken the theoretical insights obtained from such models (Allen, 2007a). Our models have smaller numbers of variables and parameters with equally predicting capability compared with complex

computational models. This feature allows advance mathematical analysis to reveal robust dynamical behaviours for the underlying mechanisms in theoretical biology.

Finally, we recognize the limitations of this work. It is unknown whether the levels of noise present in the simulation results reflect the levels of demographic and environmental noise in the lung. Future studies may be needed to examine this and, if the levels are considerably different, then alterations to the model may be necessary. Moreover, in future work, we will consider altering the ODE model, such as adjusting the rates of the infected-induced T-cell proliferation to saturate with the concentration of infected macrophages and Mtb bacteria.

Acknowledgements

The author would like to express her appreciation to Dr. Linda Allen from Texas Tech University for her comments and suggestions on the stochastic formulation and simulation. Special thanks are also extended to Dr Leif Ellingson from Texas Tech University for his help with carefully editing the paper. The author also thanks both referees for their comments and suggestions, which are very helpful for improving the manuscript.

Funding

The author acknowledges the generous support from Simons Foundation Collaboration Grants for Mathematicians (A21-0013-001).

References

Alexander, H. & Wahl, L. M. (2011) Self-tolerance and autoimmunity in a regulatory t cell model. *Bull. Math. Biol.*, **73**, 33–71.

Allen, E. (1999) Stochastic differential equations and persistence time for two interacting populations. *Dyn. Contin. Discrete Impuls. Syst.*, **5**, 271–281.

Allen, E. (2007a) *Modeling with Itô Stochastic Differential Equations*, vol. 22. New York: Springer Science & Business Media.

Allen, E., Allen, L. & Smith, H. (2020) On real-valued SDE and nonnegative-valued SDE population models with demographic variability. *J. Math. Biol.*, **81**, 487–515.

Allen, E. J., Allen, L. J., Arciniega, A. & Greenwood, P. E. (2008) Construction of equivalent stochastic differential equation models. *Stoch. Anal. Appl.*, **26**, 274–297.

Allen, L. J. (2007b) *An Introduction to Mathematical Biology*. Pearson/Prentice Hall.

Allen, L. J. (2010) *An Introduction to Stochastic Processes with Applications to Biology*. Boca Raton, FL: CRC Press.

Allen, L. J. (2017) A primer on stochastic epidemic models: formulation, numerical simulation, and analysis. *Infect. Dis. Model.*, **2**, 128–142.

Antony, V. B., Godbey, S. W., Kunkel, S. L., Hott, J. W., Hartman, D. L., Burdick, M. D. & Strieter, R. M. (1993) Recruitment of inflammatory cells to the pleural space. Chemotactic cytokines, il-8, and monocyte chemotactic peptide-1 in human pleural fluids. *J. Immunol.*, **151**, 7216–7223.

Arranz-Trullén, J., Lu, L., Pulido, D., Bhakta, S. & Boix, E. (2017) Host antimicrobial peptides: the promise of new treatment strategies against tuberculosis. *Front. Immunol.*, **8**, 1499.

Bark, C. M., Manceur, A. M., Malone, L. L., Nsereko, M., Okware, B., Mayanja, H. K., Joloba, M. L., Rajotte, I., Mentinova, M., Kay, P., et al. (2017) Identification of host proteins predictive of early stage mycobacterium tuberculosis infection. *EBioMedicine*, **21**, 150–157.

Behar, S., Martin, C., Booty, M., Nishimura, T., Zhao, X., Gan, H., Divangahi, M. & Remold, H. (2011) Apoptosis is an innate defense function of macrophages against mycobacterium tuberculosis. *Mucosal Immunol.*, **4**, 279–287.

Bisset, L. R., Lung, T. L., Kaelin, M., Ludwig, E. & Dubs, R. W. (2004) Reference values for peripheral blood lymphocyte phenotypes applicable to the healthy adult population in Switzerland. *Eur. J. Haematol.*, **72**, 203–212.

Chakraborti, C. K. (2011) Vitamin D as a promising anticancer agent. *Indian J. Pharm.*, **43**, 113.

Cobat, A., Gallant, C. J., Simkin, L., Black, G. F., Stanley, K., Hughes, J., Doherty, T. M., Hanekom, W. A., Eley, B., Jaïs, J.-P. & Boland-Auge, A. (2009) Two loci control tuberculin skin test reactivity in an area hyperendemic for tuberculosis. *J. Exp. Med.*, **206**, 2583–2591.

Cohen, A., Mathiasen, V. D., Schön, T. & Wejse, C. (2019) The global prevalence of latent tuberculosis: a systematic review and meta-analysis. *Eur. Respir. J.*, **54**, 1–14.

Conde, M. B. & Lapa e Silva, J. R. (2011) New regimens for reducing the duration of treatment of drug-susceptible pulmonary tuberculosis. *Drug Dev. Res.*, **72**, 501–508.

de Martino, M., Lodi, L., Galli, L. & Chiappini, E. (2019) Immune response to mycobacterium tuberculosis: a narrative review. *Front. Pediatr.*, **7**, 350.

Dhooge, A., Govaerts, W. & Kuznetsov, Y. A. (2003) Matcont: a MATLAB package for numerical bifurcation analysis of ODEs. *ACM Trans. Math. Softw.*, **29**, 141–164.

Du, Y., Wu, J. & Heffernan, J. M. (2017) A simple in-host model for mycobacterium tuberculosis that captures all infection outcomes. *Math. Popul. Stud.*, **24**, 37–63.

Fabri, M., Stenger, S., Shin, D.-M., Yuk, J.-M., Liu, P. T., Realegeno, S., Lee, H.-M., Krutzik, S. R., Schenk, M., Sieling, P. A. & Teles, R. (2011) Vitamin d is required for IFN-γ–mediated antimicrobial activity of human macrophages. *Sci. Transl. Med.*, **3**, 104ra102–104ra102.

Gammack, D., Ganguli, S., Marino, S., Segovia-Juarez, J. & Kirschner, D. E. (2005) Understanding the immune response in tuberculosis using different mathematical models and biological scales. *Multiscale Model. Simul.*, **3**, 312–345.

Gombart, A. F. (2009) The vitamin d–antimicrobial peptide pathway and its role in protection against infection. *Future Microbiol.*, **4**, 1151–1165.

Gupta, K. B., Gupta, R., Atreja, A., Verma, M. & Vishvkarma, S. (2009) Tuberculosis and nutrition. *Lung India*, **26**, 9.

Hasegawa, A., Liu, H., Ling, B., Borda, J. T., Alvarez, X., Sugimoto, C., Vinet-Oliphant, H., Kim, W.-K., Williams, K. C., Ribeiro, R. M. & Lackner, A. A. (2009) The level of monocyte turnover predicts disease progression in the macaque model of aids. *Blood*, **114**, 2917–2925.

Lin, P. L. & Flynn, J. A. L. (2010) Understanding latent tuberculosis: a moving target. *J. Immunol.*, **185**, 15–22.

Liu, P. T., Stenger, S., Li, H., Wenzel, L., Tan, B. H., Krutzik, S. R., Ochoa, M. T., Schauber, J., Wu, K., Meinken, C. & Kamen, D. L. (2006) Toll-like receptor triggering of a vitamin d-mediated human antimicrobial response. *Science*, **311**, 1770–1773.

Marino, S. & Kirschner, D. E. (2004) The human immune response to mycobacterium tuberculosis in lung and lymph node. *J. Theor. Biol.*, **227**, 463–486.

Martineau, A. R., Wilkinson, K. A., Newton, S. M., Floto, R. A., Norman, A. W., Skolimowska, K., Davidson, R. N., Sørensen, O. E., Kampmann, B., Griffiths, C. J., et al. (2007) Ifn-γ-and tnf-independent vitamin d-inducible human suppression of mycobacteria: the role of cathelicidin ll-37. *J. Immunol.*, **178**, 7190–7198.

Meermeier, E. W. & Lewinsohn, D. M. (2018) Early clearance versus control: what is the meaning of a negative tuberculin skin test or interferon-gamma release assay following exposure to mycobacterium tuberculosis? *F1000Research*, **7**.

Meng, Y., Lai, Y.-C. & Grebogi, C. (2020) Tipping point and noise-induced transients in ecological networks. *J. R. Soc. Interface*, **17**, 20200645.

Mitnick, C. D., McGee, B. & Peloquin, C. A. (2009) Tuberculosis pharmacotherapy: strategies to optimize patient care. *Expert. Opin. Pharmacother.*, **10**, 381–401.

Naranbhai, V., Hill, A., Abdool Karim, S., Naidoo, K., Abdool Karim, Q., Warimwe, G. M., McShane, H. & Fletcher, H. (2013) Blood monocyte-lymphocyte ratios identify adults at risk of incident tuberculosis amongst patients initiating antiretroviral therapy. *J. Infect. Dis.*, **209**, 500–509.

Perelson, A. S. & Nelson, P. W. (1999) Mathematical analysis of hiv-1 dynamics *in vivo*. *SIAM Rev.*, **41**, 3–44.

Rosenberger, C. M., Gallo, R. L. & Finlay, B. B. (2004) Interplay between antibacterial effectors: a macrophage antimicrobial peptide impairs intracellular salmonella replication. *Proc. Natl. Acad. Sci.*, **101**, 2422–2427.

Schwander, S. K., Torres, M., Sada, E., Carranza, C., Ramos, E., Tary-Lehmann, M., Wallis, R. S., Sierra, J. & Rich, E. A. (1998) Enhanced responses to mycobacterium tuberculosis antigens by human alveolar lymphocytes during active pulmonary tuberculosis. *J. Infect. Dis.*, **178**, 1434–1445.

Schwartz, N. G., Price, S. F., Pratt, R. H. & Langer, A. J. (2020) Tuberculosis-United States, 2019. *Morb. Mortal. Wkly Rep.*, **69**, 286.

Smith, I. (2003) Mycobacterium tuberculosis pathogenesis and molecular determinants of virulence. *Clin. Microbiol. Rev.*, **16**, 463–496.

Sud, D., Bigbee, C., Flynn, J. L. & Kirschner, D. E. (2006) Contribution of CD8+ T cells to control of mycobacterium tuberculosis infection. *J. Immunol.*, **176**, 4296–4314.

The Editors of Encyclopaedia Britannica (2022) Streptomycin. https://www.britannica.com/science/streptomycin. Encyclopedia Britannica (1 July 2013 date last accessed).

Tobin, D. M. (2015) Host-directed therapies for tuberculosis. *Cold Spring Harb. Perspect. Med.*, **5**, a021196.

Uplekar, M., Weil, D., Lonnroth, K., Jaramillo, E., Lienhardt, C., Dias, H. M., Falzon, D., Floyd, K., Gargioni, G., Getahun, H. & Gilpin, C. (2015) WHO's new end TB strategy. *The Lancet*., **385**, 1799–1801.

Wheelwright, M., Kim, E. W., Inkeles, M. S., De Leon, A., Pellegrini, M., Krutzik, S. R. & Liu, P. T. (2014) All-trans retinoic acid–triggered antimicrobial activity against mycobacterium tuberculosis is dependent on npc2. *J. Immunol.*, **192**, 2280–2290.

Wigginton, J. E. & Kirschner, D. (2001) A model to predict cell-mediated immune regulatory mechanisms during human infection with mycobacterium tuberculosis. *J. Immunol.*, **166**, 1951–1967.

Wodarz, D. (2007) *Killer Cell Dynamics Mathematical and Computational Approaches to Immunology*. New York: Springer.

World Health Organization, et al. (2020) *WHO consolidated guidelines on tuberculosis: tuberculosis preventive treatment*. World Health Organization

Yu, P. (2005) Closed-form conditions of bifurcation points for general differential equations. *Int. J. Bifur. Chaos*, **15**, 1467–1483.

Zhang, W. (2020) Analysis of an in-host tuberculosis model for disease control. *Appl. Math. Lett.*, **99**, 105983.

Zhang, W., Ellingson, L., Frascoli, F. & Heffernan, J. (2021) An investigation of tuberculosis progression revealing the role of macrophages apoptosis via sensitivity and bifurcation analysis. *J. Math. Biol.*, **83**, 1–32.

Zhang, W., Frascoli, F. & Heffernan, J. M. (2020) Analysis of solutions and disease progressions for a within-host tuberculosis model. *Math. Appl. Sci. Eng.*, **1**, 39–49.

Zhang, W., Wahl, L. M. & Yu, P. (2014) Viral blips may not need a trigger: how transient viremia can arise in deterministic in-host models. *SIAM Rev.*, **56**, 127–155.

Zumla, A., Chakaya, J., Hoelscher, M., Ntoumi, F., Rustomjee, R., Vilaplana, C., Yeboah-Manu, D., Rasolofo, V., Munderi, P., Singh, N. & Aklillu, E. (2015) Towards host-directed therapies for tuberculosis. *Nat. Rev. Drug Discov.*, **14**, 511–512.

Zumla, A., Ippolito, G., Ntoumi, F., Seyfert-Margolies, V., Nagu, T. J., Cirillo, D., Chakaya, J. M., Marais, B. & Maeurer, M. (2020) Host-directed therapies and holistic care for tuberculosis. *Lancet Respir. Med.*, **8**, 337–340.